Biophysical Journal
Article

Biophysical Society

Molecular Determinants of Substrate Affinity and Enzyme Activity of a Cytochrome $P450_{BM3}$ Variant

Inacrist Geronimo,[1] Catherine A. Denning,[2] David K. Heidary,[2] Edith C. Glazer,[2,*] and Christina M. Payne[1,*]
[1]Department of Chemical and Materials Engineering and [2]Department of Chemistry, University of Kentucky, Lexington, Kentucky

ABSTRACT Cytochrome $P450_{BM3}$ catalyzes the hydroxylation and/or epoxidation of fatty acids, fatty amides, and alcohols. Protein engineering has produced $P450_{BM3}$ variants capable of accepting drug molecules normally metabolized by human P450 enzymes. The enhanced substrate promiscuity has been attributed to the greater flexibility of the lid of the substrate channel. However, it is not well understood how structurally different and highly polar drug molecules can stably bind in the active site nor how the activity and coupling efficiency of the enzyme may be affected by the lack of enzyme-substrate complementarity. To address these important aspects of non-native small molecule binding, this study investigated the binding of drug molecules with different size, charge, polar surface area, and human P450 affinity on the promiscuous R47L/F87V/L188Q/E267V/F81I pentuple mutant of $P450_{BM3}$. Binding free energy data and energy decomposition analysis showed that pentuple mutant $P450_{BM3}$ stably binds (i.e., negative ΔG_b°) a broad range of substrate and inhibitor types because dispersion interactions with active site residues overcome unfavorable repulsive and electrostatic effects. Molecular dynamics simulations revealed that 1) acidic substrates tend to disrupt the heme propionate A-K69 salt bridge, which may reduce heme oxidizing ability, and 2) the lack of complementarity leads to high substrate mobility and water density in the active site, which may lead to uncoupling. These factors must be considered in future developments of $P450_{BM3}$ as a biocatalyst in the large-scale production of drug metabolites.

INTRODUCTION

Characterization of the metabolite profile of a drug candidate is a crucial part of the drug discovery and development process. Drug metabolites, largely produced by hepatic cytochrome P450 enzymes (P450s), are needed as reference compounds and reactive intermediates for assessing toxicity, drug-drug interactions, and biological activity (1,2). For the preparative-scale synthesis of human drug metabolites, CYP102A1 ($P450_{BM3}$), a fatty acid hydroxylase from *Bacillus megaterium*, is considered an ideal biocatalyst because it has the highest known monooxygenase activity among P450s, is relatively stable compared to human P450s, and can be expressed at high levels in *Escherichia coli* (3–5). Wild-type (WT) $P450_{BM3}$ has been shown to catalyze the oxidation of nifedipine, propranolol, and chlorzoxazone, which are substrates of the human P450s CYP3A4, CYP2D6, and CYP2E1, respectively (6). To take full advantage of $P450_{BM3}$ in an industrial setting, much research has been devoted to further expanding its substrate promiscuity and chemical reactivity through protein engineering (5,7–12). However, the molecular factors responsible for the stability of substrate binding and the potential consequences of introducing non-native substrates on the activity and coupling efficiency (i.e., ratio of substrate reacted/nicotinamide adenine dinucleotide phosphate cofactor consumed (13)) of $P450_{BM3}$ have yet to be determined. Peroxide or oxidase uncoupling (Fig. 1) is of particular concern because it prevents product formation, thereby wasting reducing equivalents from the expensive nicotinamide adenine dinucleotide phosphate cofactor (14,15).

Interestingly, the $P450_{BM3}$ variants developed to metabolize additional drug classes (e.g., nonsteroidal anti-inflammatory drugs like diclofenac, ibuprofen, and naproxen), including D251G/Q307H (16,17), RP/FV/EV/FW (7), RT2/AP/FW (7), M11 (9–11), and W7D8 (12) (Table 1), do not share common substitutions. However, the mutations, generally located far from the heme active site, appear to have a similar functional effect of increasing the flexibility of the lid domain (helices B′, F, and G, Fig. 2), as revealed by the unresolved (or very high B factors of) lid domain residues in the crystal structures of the substrate-free variants (7,11,12,17–19). Molecular dynamics simulations of the R47L/F87V/L188Q/E267V/F81I pentuple mutant (PM) showed that the lid domain is indeed highly labile and consequently one of the regions

Submitted July 2, 2018, and accepted for publication August 20, 2018.
*Correspondence: ec.glazer@uky.edu or christy.payne@uky.edu
Editor: Alan Grossfield.
https://doi.org/10.1016/j.bpj.2018.08.026

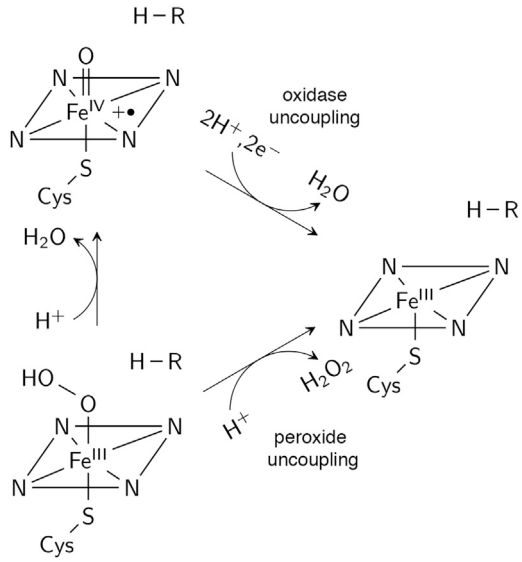

FIGURE 1 Peroxide and oxidase uncoupling pathways. The substrate is represented by R-H. The oxoferryl porphyrin radical intermediate is the species presumed to oxidize the substrate.

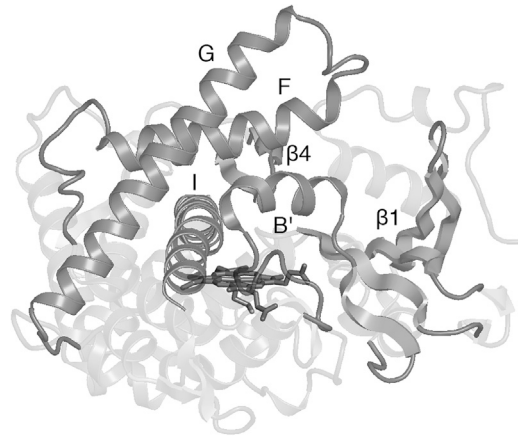

FIGURE 2 $P450_{BM3}$ structure. Regions involved in substrate binding, including the lid domain (helices B′, F, and G), are labeled in the figure. Heme is shown as sticks.

that first unfolds at high temperature (20). In the cases of D251G/Q307H (Protein Data Bank (PDB): 5DYP (17)), M11 (PDB: 5E9Z (11)), and RP/FV/EV (PDB: 4RSN (7)), the cause of increased flexibility is evident: D251 and E267 are part of the region that moves during the opening and closing of the substrate channel and form salt bridges with K224 and K440, respectively, in WT (21,22). The higher flexibility of the lid domain would account for the ability of $P450_{BM3}$ variants to accept a broader range of substrates (12,18). The crystal structures further showed that substrate-free variants adopt the closed conformation characteristic of substrate-bound WT instead of the open conformation. This shift to the catalytically "ready" conformation caused by mutation results in a more positive heme reduction potential. Consequently, the rate of the first electron transfer (believed to be the rate-limiting step (23)) increases, improving the oxidative activity of $P450_{BM3}$ toward non-native substrates (7,16,17,19,24).

TABLE 1 List of Mutations in Functional $P450_{BM3}$ Variants

Variant	Mutations
RP/FV/EV (7)	R47L/Y51F/F87V/E267V/I401P
RP/FV/EV/FW (7)	RP/FV/EV/F81W
RT2/AP/FW (7)	R47L/Y51F/A191T/N239H/I259V/A276T/L353I/A330P/F81W
M01 (8)	R47L/F87V/L188Q/E267V/G415S
M02 (8)	R47L/L86I/F87V/L188Q/N319T/A964V
M05 (8)	M01/F81I/G1049E
M11 (9–11)	M01/E64G/F81I/E143G/Y198C/H285Y
MT35 (10)	M11/L437S
W7D8 (12)	L52I/I58V/L75R/L86L/F87A/H100R/S106R/F107L/Q109L/A135S/E140G/F162I/A184V/N239H/S274T/L324I/V340M/I366V/K434E/E442K/V446I
9-10A (5)	V78A/H138Y/T175I/V178I/A184V/H236Q/E252G/R255S/A290V/A295T/L353V/Y138H/I178V/F205C/S226R/A290V/R47C/K94I/P142S

The only crystal structures of drug-bound $P450_{BM3}$ variants that have been reported thus far are A82F and A82F/F87V with omeprazole (PDB: 4KEW and 4KEY (18)), A82F/F87V with esomeprazole (PDB: 4O4P (25)), and PM with metyrapone (PDB: 4ZF8 (20)). In all structures, the conformation is notably similar to that of the WT fatty acid complex (PDB: 1FAG (26)), raising two important questions: 1) what interactions stabilize a structurally different and highly polar drug molecule in the largely hydrophobic active site and 2) how would the lack of structural and electrostatic complementarity between substrate and enzyme affect activity and coupling efficiency? This study aims to address these key mechanistic questions by investigating the binding of a set of drugs of varying size, charge, polar surface area, and human P450 affinity. PM $P450_{BM3}$ was chosen as the model system because it serves as a good platform to develop biocatalysts for the synthesis of drug metabolites as well as for diversification of lead compounds; this was demonstrated by a study in which a library of mutants containing the PM mutations was able to metabolize 77% of the 43 commercial drugs tested by more than 20% (10).

The binding free energies of CYP2C9 (diclofenac, naproxen, and *S*-warfarin), CYP2D6 (astemizole, dextromethorphan, and 3,4-methylenedioxymethamphetamine or MDMA), and CYP2A6 (nicotine and cotinine) substrates,

CYP2C9 inhibitors (lovastatin and *R*-warfarin), and metyrapone (Fig. 3; Table S1) were determined using spectral binding titrations and supported by calculations using free-energy perturbation with Hamiltonian replica-exchange molecular dynamics (FEP/λ-REMD). To gain insight on the nature of the interaction that enables the binding of non-native small molecules in the $P450_{BM3}$ mutant, the calculated free energy was further decomposed into repulsive, dispersive, and electrostatic contributions. Residues that play a role in substrate binding were identified by analyzing hydrogen bond, ionic, and van der Waals interactions from the molecular dynamics (MD) trajectories. The possibility of reduced heme oxidizing ability and uncoupling caused by the binding of non-native substrates was assessed by examining electrostatic interactions and water density in the active site.

MATERIALS AND METHODS

Chemicals

Dextromethorphan hydrobromide monohydrate, metyrapone, and sodium palmitate (palmitic acid) were purchased from Sigma Aldrich (St. Louis, MO). (-)-Cotinine, lovastatin, and naproxen sodium were purchased from Alfa Aesar (Haverhill, MA). Nicotine and warfarin sodium were purchased from TCI America (Portland, OR).

Cloning and site-directed mutagenesis of $P450_{BM3}$

The heme domain of $P450_{BM3}$ (Thr 1-Thr 463) with a C-terminal 6xHis tag was cloned into the pCWori plasmid. Mutations for generating PM $P450_{BM3}$ were incorporated using QuikChange site-directed mutagenesis (Stratagene, San Diego, CA). The polymerase chain reaction product was DpnI treated, transformed into XL-Gold ultracompetent cells, and selected on carbenicillin Luria Broth (LB)-agar plates. Colonies were grown in 5 mL of LB with 100 μg/mL ampicillin, followed by plasmid isolation using the E.Z.N.A. Plasmid Mini Kit (Omega Bio-tek, Norcross, GA). All mutations were confirmed by sequence analysis.

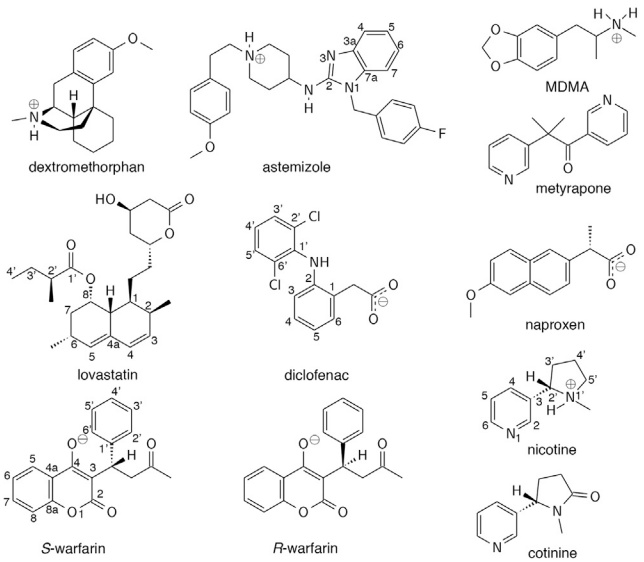

FIGURE 3 Drug molecules included in the study.

Expression and purification of PM $P450_{BM3}$

The pCWori vector containing the PM $P450_{BM3}$ heme domain was transformed in *E. coli* BL21(DE3) cells. Colonies were grown overnight in 5 mL LB with 100 μg/mL ampicillin in an incubator set to 190 rotations per minute and 37°C before being transferred to 1 L Terrific Broth supplemented with 8 mL of 80% glycerol and 100 μg/mL ampicillin. The cells were grown until an optical density at 600 nm of 0.7–0.8 was reached. Expression of PM $P450_{BM3}$ was induced upon addition of isopropyl β-D-1-thiogalactopyranoside at a final concentration of 0.5 mM. Cells were harvested after ~16 h by centrifugation at 4°C and 3000 *g* for 15 min. The cell pellets were stored at −80°C before purification.

Cell pellets were resuspended in 30 mL lysis buffer (50 mM NaH_2PO_4, 300 mM NaCl, 10 mM imidazole, 0.1 mM EDTA (pH 8.0)) with 0.1 mM phenylmethylsulfonyl fluoride. Cells were lysed on ice for 15 min by a microtip sonifier with an output control of 3 and duty cycle of 50% (Sonifier 250; Branson Ultrasonics, Danbury, CT). The lysate was centrifuged at 4°C and 17,000 *g* for 1 h; the supernatant was decanted and filtered through a 0.45 μM polytetrafluoroethylene filter.

The clarified lysate was loaded onto a His-Trap column (GE Healthcare, Chicago, IL) equilibrated with buffer A (50 mM NaH_2PO_4, 300 mM NaCl, 10 mM imidazole), and the protein was eluted with a linear gradient with buffer B (50 mM NaH_2PO_4, 300 mM NaCl, 200 mM imidazole), in which the concentration increased from 10 to 200 mM imidazole. Fractions containing PM $P450_{BM3}$ were collected and concentrated to ~2 mL at 4500 *g* and 4°C with Ultracel-30K Millipore (Burlington, MA) centrifugal units. The concentrated protein was loaded onto a Hi-Prep 26/60 Sephacryl S200 HR size exclusion column (GE Healthcare, Pittsburgh, PA) equilibrated with 20 mM Tris and 150 mM NaCl buffer at pH 8.0. Fractions containing PM $P450_{BM3}$ were analyzed by absorbance spectroscopy, and all fractions with a spectrophotometric index (A_{420}/A_{280}) above 1.2 were combined and concentrated. The protein concentration was determined by CO binding (ε = 91,000 M^{-1} cm^{-1}) (27). Glycerol was added to ~50%, with the final protein concentration between 15 and 20 mg/mL. The protein was aliquoted, snap frozen in a dry ice ethanol bath, and stored at −80°C until use.

Binding constant determination by spectral titration

Dextromethorphan hydrobromide monohydrate, naproxen sodium, nicotine, and warfarin sodium stock solutions were prepared in 18.2 MΩ water. (-)-Cotinine, lovastatin, metyrapone, and palmitic acid were prepared in dimethyl sulfoxide. Ultraviolet/visible absorption spectra were recorded using an Agilent 8453 (Agilent Technologies, Santa Clara, CA) spectrophotometer. Titrations were carried out in 2 mL of 100 mM KH_2PO_4 (pH 7.4) in a 1-cm optical pathlength cuvette, with protein concentrations between 0.15 and 0.25 mg/mL. All titrations were carried out with the organic solvent concentration kept below 1%.

Difference spectra were generated by subtracting the absorption spectrum at each concentration point in the titration from the original compound-free $P450_{BM3}$ absorption spectrum. The wavelength in which the maximal change occurred was identified and used to determine the apparent dissociation constant (K_d), which was calculated in GraphPad Prism version 6 by fitting the data for the ligand-induced absorbance changes in the difference spectra ($A_{max} - A_{min}$) versus ligand concentration to a quadratic equation. The ΔG_b° value was determined using the equation $\Delta G_b^\circ = -RT \ln K_d$, where R = 1.99 × 10^{-3} kcal K^{-1} mol^{-1} and T = 298.15 K. A full spin shift was obtained using omeprazole as the substrate. For all other ligands, the percentage of protein in the high-spin state was calculated

based on the assumption that water-bound PM $P450_{BM3}$ is 100% low spin and PM $P450_{BM3}$ fully bound to omeprazole is 100% high spin (Fig. S1).

MD simulations

Initial coordinates for the PM-metyrapone complex were obtained from the crystal structure (PDB: 4ZF8) (20). The other enzyme-substrate complexes were prepared by ligand docking using AutoDock 4.2 (28). The structure of the solvent-free target protein (including the heme) was taken from the last point of the 100-ns, fully atomistic simulation of the PM-metyrapone complex performed in a previous study (20). The charges used for the protein atoms were the same as the ones used in the MD simulation, and ligand charges were calculated using the restrained electrostatic potential method (vide infra) (29). The size of the grid box centered on the Fe atom was 60 × 60 × 60 Å, with a spacing of 0.250 Å. During the docking simulations, the protein was kept rigid, whereas all rotatable dihedrals in the ligands were allowed to move freely. The Lamarckian genetic algorithm was used to search for low-energy ligand poses that will yield the metabolites known to be produced by human P450s and/or $P450_{BM3}$ mutants containing the PM mutations.

Preparation of the enzyme-substrate complexes for MD simulations, including assignment of the protonation state of titratable residues, has been described in detail in (20). The solvated ligand system was prepared by neutralizing the ligand with Na^+ or Cl^- and solvating it in a truncated octahedron box of transferable intermolecular potential with 3 points water (30) with a buffer distance of 25 Å between each wall and the closest atom in each direction. The AMBER ff14SB force field (31) was used to describe the protein. Force field parameters and partial charges for the high-spin, pentacoordinate ferric form of the heme active site (characteristic of substrate-bound $P450_{BM3}$ (22)) were taken from literature (32). These parameters have been tested for stability and consistency with the expected heme geometry in implicit and explicitly solvated MD simulations of the heme active site alone and CYP3A4. Moreover, the use of the partial charges in docking calculations reproduced the experimentally observed metabolism of raloxifene by CYP3A4 (32). Ligand parameters were calculated using antechamber (33) at the Hartree-Fock/6-31G* level to be consistent with the GAFF force field (34). These are provided as Supporting Material. Periodic boundary conditions were applied using the particle mesh Ewald method (35) with a nonbonded cutoff of 10 Å. Energy minimization was performed in four stages: 1) protein and ligand were restrained with a harmonic force constant of 5.0 kcal/mol/Å^2 to allow water and ions to relax, 2) residues within 5 Å of the docked ligand were released from the restraint, 3) the whole protein was again restrained while the ligand was allowed to relax, and 4) the restraint was removed. At each stage, 1000 steps of steepest descent minimization were performed, followed by 1000 steps of conjugate gradient minimization.

The system was then heated from 0 to 300 K for 50 ps using NMR weight restraints to linearly increase the temperature (~6 K/ps) to avoid instabilities in the simulation. Cα atoms were restrained with a harmonic force constant of 5.0 kcal/mol/Å^2 during heating. Bonds involving hydrogen were constrained using the SHAKE algorithm (36), and a 2-fs time step was used for time integration. The temperature was controlled using Langevin dynamics (37) with a collision frequency of 1.0 ps^{-1}. The system was equilibrated at constant pressure over a 200-ps period, during which the force constant was incrementally reduced (5.0, 2.0, 1.0, and 0.5 kcal/mol/Å^2). Isotropic position scaling was used to maintain the pressure at 1 atm, with a relaxation time of 2 ps. Equilibration of the unrestrained system was then continued for 2 ns. Production MD simulations in the NVT ensemble were performed at 300 K for 100 ns using the same parameters as equilibration. During production, a harmonic restraint of 10 kcal/mol/Å was applied to the distance between the heme Fe and protonated nitrogen of dextromethorphan and MDMA to prevent large displacement of the substrate due to strong ionic interaction with heme propionate A.

Minimization, heating, and equilibration were run using Amber 14 (38) and production using nanoscale molecular dynamics (39). Residue-ligand interaction energies were calculated using nanoscale molecular dynamics (Tables S1, S2, and S3). Hydrogen bond occupancy (i.e., fraction of time that the bond is present in each trajectory) and water density around the ligand and heme were calculated using the *cpptraj* module of Amber 2015 (40,41). The distance and angle cutoffs for the hydrogen bond are 3.0 Å and 135° (Tables S4 and S5). The grid dimensions of the ligand + heme region used in the water density calculation were determined using the "bounds" command (grid spacing = 0.5 Å). The water density was visualized with PyMOL (42) using a contour level of 3.0 and mesh width of 0.5.

FEP/λ-REMD

In the FEP/λ-REMD method (43), the binding process is divided according to the thermodynamic cycle, wherein the bound ligand is decoupled from the enzyme (Eq. 1) and the solvated ligand is decoupled from bulk solution (Eq. 2). The free energy for the overall process (Eq. 3) is $\Delta G_b^\circ = \Delta G_2 - \Delta G_1$.

$$Enzyme \times Ligand_{solv} \xrightarrow{\Delta G_1} Enzyme_{solv} + Ligand_{vac} \quad (1)$$

$$Ligand_{solv} \xrightarrow{\Delta G_2} Ligand_{vac} \quad (2)$$

$$Enzyme_{solv} + Ligand_{solv} \xrightarrow{\Delta G_b^\circ} Enzyme \times Ligand_{solv} \quad (3)$$

The ligand is decoupled from the binding pocket or bulk solution in three stages using the thermodynamic coupling parameters λ_{rep}, λ_{disp}, and $\lambda_{elec} \in [0,1]$ (Eqs. 4, 5, and 6), giving the repulsive (ΔG_{rep}), dispersive (ΔG_{disp}), and electrostatic (ΔG_{elec}) contributions, respectively.

$$U(\lambda_{rep} = 0, \lambda_{disp} = 0, \lambda_{elec} = 0, \lambda_{rstr} = 1) \rightarrow U(\lambda_{rep} = 1, \lambda_{disp} = 0, \lambda_{elec} = 0, \lambda_{rstr} = 1) \quad (4)$$

$$U(\lambda_{rep} = 1, \lambda_{disp} = 0, \lambda_{elec} = 0, \lambda_{rstr} = 1) \rightarrow U(\lambda_{rep} = 1, \lambda_{disp} = 1, \lambda_{elec} = 0, \lambda_{rstr} = 1) \quad (5)$$

$$U(\lambda_{rep} = 1, \lambda_{disp} = 1, \lambda_{elec} = 0, \lambda_{rstr} = 1) \rightarrow U(\lambda_{rep} = 1, \lambda_{disp} = 1, \lambda_{elec} = 1, \lambda_{rstr} = 1) \quad (6)$$

For the decoupling of the bound ligand from the enzyme, an additional parameter, λ_{rstr}, is used to control the translational and orientational restraints (Eq. 7) and gives ΔG_{rstr}.

$$U(\lambda_{rep} = 1, \lambda_{disp} = 1, \lambda_{elec} = 1, \lambda_{rstr} = 1) \rightarrow U(\lambda_{rep} = 1, \lambda_{disp} = 1, \lambda_{elec} = 1, \lambda_{rstr} = 0) \quad (7)$$

The initial structure for the enzyme-substrate complex was taken from the 25-ns snapshot of the production MD simulation, whereas that for the solvated ligand was taken from the last point of the equilibration. The same simulation parameters outlined above were used except for the time step, which was reduced to 1 fs. Nonbonded forces were evaluated every step and full electrostatic forces every other step. A harmonic restraint was applied with a force constant of 10.0 kcal/mol/Å^2 to maintain the center-of-mass distance between the ligand and enzyme. 128 replicas (72 repulsive, 24 dispersive, and 32 electrostatic) were used with an exchange frequency of 1/100 steps. Sequential 0.1-ns simulations were performed

until the calculation converged (at least 2 ns), as evaluated from the fluctuation in the absolute free energy of the system over time (Fig. S2). Repulsive, dispersive, and electrostatic contributions were determined using the multistate Bennett acceptance ratio method (44). The average and standard deviation of the binding free energy were calculated using the last 1 ns of data.

RESULTS AND DISCUSSION

Experimental and calculated binding free energies

Substrate binding displaces the water molecule coordinated to the sixth position of the heme iron, resulting in a type I shift in the absorption spectrum, with the peak at ~390 nm in the difference spectra (45). The native substrate, palmitic acid, as well as diclofenac, naproxen, warfarin (the racemic mixture), lovastatin, and dextromethorphan exhibited a type I spectral shift upon binding (Figs. 4 and S3). In the case of warfarin, the type I binding observed is presumably that of *S*-warfarin, as the *R* enantiomer is known to be inhibitory and would bind in a nonproductive manner that does not lead to metabolism (46). Displacement of the water ligand changes the iron spin state from low to high spin and consequently alters the redox potential of the heme (47). The population of the high-spin state for PM P450$_{BM3}$ upon drug binding was lower than that observed with palmitic acid (Table 2), suggesting that the drug molecules possibly bind in the active site without displacing the water ligand in a fraction of the protein (48). A type II spectral shift occurred with metyrapone, nicotine, and cotinine, as evidenced by the absorption shift to ~430–455 nm (Figs. 4 and S3) (45). The type II shift indicates that these compounds directly coordinated to the heme iron through the pyridine nitrogen. Generally, the type II shift is associated with enzyme inhibition; nevertheless, with nicotine or cotinine bound, the enzyme was active, as metabolism was observed using the fluorescence-based 7-ethoxyresorufin-O-deethylase activity assay (Fig. S4) (49).

The binding affinity of various drug molecules for PM P450$_{BM3}$ was determined upon titrating small molecules and quantifying the change in absorption to obtain their K_d values. Based on predicted titration curves, diclofenac, naproxen, and warfarin are acidic; dextromethorphan and nicotine are basic; and cotinine, lovastatin, and metyrapone are neutral at physiological pH (Table S1). All substrates have negative ΔG_b°, indicating that binding to PM P450$_{BM3}$ is stable, regardless of the type of drug (acidic, basic, or neutral) (Table 2). Moreover, the binding affinities of naproxen, warfarin, dextromethorphan, and lovastatin are comparable to that of palmitic acid. Cotinine was the weakest binder, as indicated by the largest K_d value (415 μM), ~20× higher than that of nicotine (23.5 μM). The two molecules have the same ring systems, but unlike nicotine, cotinine has an additional carbonyl group and is neutral. The binding free energies calculated using FEP/λ-REMD agree with experimental data for diclofenac, lovastatin, and dextromethorphan (Table 2). *S*-warfarin has a sixfold higher affinity than its enantiomer, and the calculated ΔG_b° is closer to the experimental value for the racemic mixture. On the other hand, the calculated ΔG_b° of naproxen is much more negative than the experimental value, possibly because of overestimation of the electrostatic contribution. As nicotine and cotinine are subject to metabolism by P450$_{BM3}$, the productive binding modes leading to metabolism were

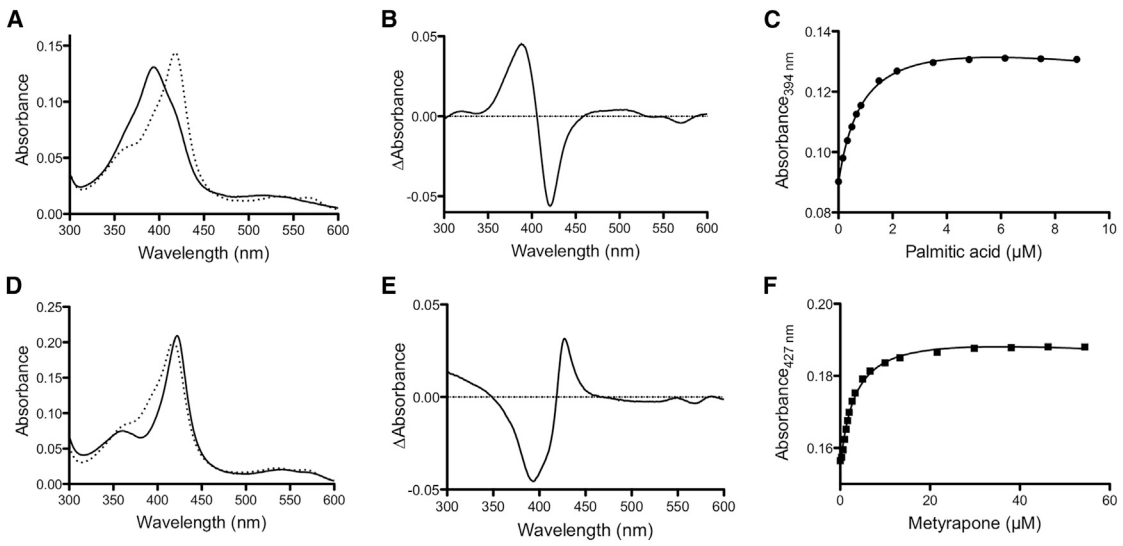

FIGURE 4 Spectral titration of PM P450$_{BM3}$ with the native substrate, palmitic acid (*A–C*), and metyrapone (*D–F*). The black solid curve corresponds to the ligand-saturated enzyme, and the dashed curve indicates the ligand-free enzyme. Palmitic acid exhibited a type I spectral shift characterized by λ_{max} at 394 nm and trough around 420 nm (*B*), whereas metyrapone exhibited a type II spectral shift characterized by λ_{max} at 427 nm and trough around 390 nm (*E*). The dissociation constant (K_d) was calculated by plotting the absorbance at λ_{max} as a function of ligand concentration (*C* and *F*). Difference spectra for the other substrates are shown in Fig. S3.

TABLE 2 High-Spin Fraction, Dissociation Constant K_d, and Binding Free Energy ΔG_b° of Palmitic Acid and Various Drug Molecules in PM $P450_{BM3}$

Substrate	% High spin	K_d (μM)	ΔG_b° (kcal/mol)	
			Experimental	Theoretical
Palmitic acid	94 ± 10	1.3 ± 0.9	−8.1 ± 0.4	ND
Diclofenac	83 ± 4	64.9 ± 3.9	−5.7 ± 0.1	−4.95 ± 0.62
Naproxen	80 ± 2	4.6 ± 2.9	−7.4 ± 0.4	−15.20 ± 0.77
S-warfarin	75 ± 3	0.7 ± 0.4	−8.4 ± 0.3	−11.44 ± 0.68
R-warfarin				−1.84 ± 0.68
Lovastatin	77 ± 3	3.3 ± 1.5	−7.5 ± 0.3	−6.15 ± 0.78
Dextromethorphan	74 ± 5	3.7 ± 1.2	−7.4 ± 0.2	−6.89 ± 0.64
MDMA	ND	ND	ND	−6.76 ± 0.57[a]
				−6.21 ± 0.42[b]
Astemizole	ND	ND	ND	−10.68 ± 0.91[a]
				−8.57 ± 0.88[b]
				−3.17 ± 0.53[c]
Nicotine[d]	ND	23.5 ± 6.3	−6.3 ± 0.2	−4.60 ± 0.66[e]
Cotinine[d]	ND	415 ± 11	−4.6 ± 0.1	−7.07 ± 0.60 [e]
Metyrapone[d]	ND	3.6 ± 0.6	−7.4 ± 0.1	−9.09 ± 0.41

ND, no data.
[a]Positioned for N-dealkylation.
[b]Positioned for O-dealkylation.
[c]Positioned for C-H hydroxylation.
[d]Type II binding mode.
[e]Calculated using productive binding mode.

modeled instead of the inhibitory type II binding mode indicated by the absorbance spectra. Cotinine was predicted to bind with higher affinity than its parent compound with this orientation, unlike the case observed via spectroscopic titration determined for the type II binding mode. The ΔG_b° of the basic substrates, MDMA and astemizole, was also calculated to compare the free energies of different binding poses. The binding poses leading to N- and O-dealkylation have comparable ΔG_b°. A much more positive ΔG_b° was obtained when astemizole is positioned for C-H hydroxylation at C6.

The repulsive, electrostatic, and dispersive energy contributions are illustrated in Fig. S5. The repulsive contribution is unfavorable (positive net energy) for the large ligands, astemizole, *S*-warfarin, and lovastatin, which could be attributed to expulsion of water and displacement of residues in the active site upon insertion of the ligand (50). On the other hand, smaller ligands, such as metyrapone, nicotine, and cotinine, have slightly favorable repulsive contribution because their small size allows binding without causing steric clashes. As expected, the electrostatic contribution generally becomes unfavorable as the ligand moves from bulk solution to the hydrophobic active site because of the loss of ligand-solvent hydrogen bonding interactions (50). Only the two acidic substrates, naproxen and *S*-warfarin, have negative net electrostatic energies. Thus, the binding of non-native substrates in PM is mainly facilitated by dispersion interactions. This contribution correlates with molecular size and compensates for the unfavorable repulsive contribution, particularly in the binding of astemizole and lovastatin.

Protein-ligand interactions in the PM $P450_{BM3}$ active site

Residues that facilitate the binding of non-native substrates were identified from analysis of the MD trajectories. The calculated average structures of the different enzyme-substrate complexes are shown in Figs. 5, 6, and 7. The discussion of the different drug molecules is divided below by the human P450s primarily responsible for their metabolism.

CYP2C9 substrates and inhibitors

CYP2C9 metabolizes ~15% of clinical drugs and exhibits selectivity toward lipophilic anions, including the nonsteroidal anti-inflammatory drugs diclofenac and naproxen and anticoagulant *S*-warfarin (51). Diclofenac yields 4′-hydroxydiclofenac upon oxidation by CYP2C9 (52); this metabolite was also obtained using $P450_{BM3}$ variants containing some or all of the mutations found in PM (e.g., RP/FV/EV (7), M11 (9), and MT35 (10); Table 1). When bound to the PM $P450_{BM3}$ binding site, diclofenac has hydrophobic interactions with L75, V87, L437, and T438 (Fig. 5; Table S2). Docking calculations predicted that the carboxylate group is hydrogen bonded to T438; however, the substrate changed position after ~12 ns of the simulation to form a hydrogen bond with S72 (Table S5). Both orientations place the C4′ atom above the heme iron, though the orientation with the S72 hydrogen bond is presumably more stable. Naproxen undergoes O-demethylation by CYP2C9 to form desmethylnaproxen (53). The RP/FV/EV variant also metabolized naproxen but at a lower conversion rate (58%) compared to diclofenac (91%) (7). The naproxen

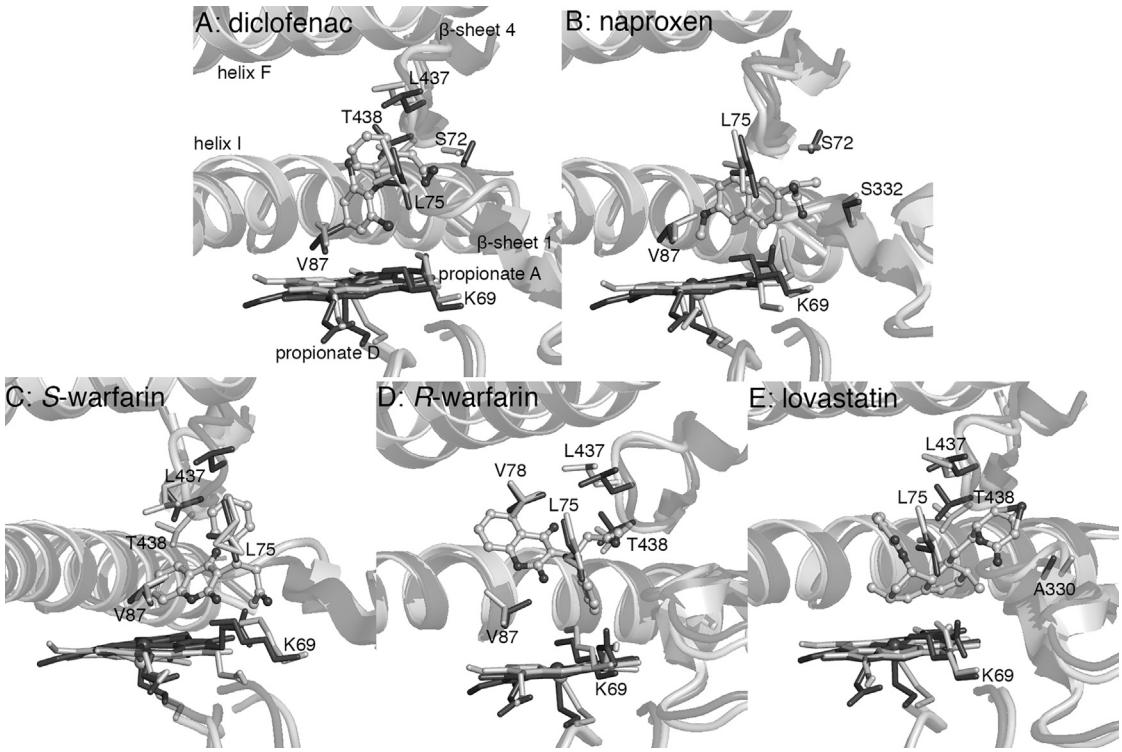

FIGURE 5 MD-averaged structures (*light gray*) superimposed on the PM-palmitic acid crystal structure (PDB: 4ZFB (20), *dark gray*). (*B*) Naproxen is positioned for O-dealkylation, whereas (*A*) diclofenac, (*C*) *S*-warfarin, (*D*) *R*-warfarin, and (*E*) lovastatin are positioned for C-H hydroxylation at C4′, C7, C4′, and C6, respectively.

hydrophobic contacts in PM are L75, V87, and A330 (Fig. 5; Table S2). As in the diclofenac complex, the carboxylate group faces the substrate channel entrance and forms not only hydrogen bonds with the hydroxyl group and backbone nitrogen of S72 and backbone nitrogen of S332, but also a salt bridge with K69 (Table S5). This facilitates a binding orientation that positions the methoxy group over the heme for O-demethylation.

S-warfarin is an acidic molecule under physiological conditions (pKa = 4.94) because of the resonance stabilization of the anion and ketone-enol tautomerization that results in delocalization of charge between O2 and O4 of the benzopyran ring. It is hydroxylated at C7 by CYP2C9 (54). In PM, it is positioned for reaction at C7 because of hydrophobic interactions primarily with L75, V87, and L437 (Fig. 5; Table S2), whereas the oxo substituent in the benzopyran ring also forms a hydrogen bond with K69 (Table S5). There was no interaction with S72. The less potent *R*-warfarin is known to competitively inhibit the metabolism of its enantiomer (46). It is positioned for C4′ attack in PM, which will yield the observed CYP2C9 product (55). Unlike its enantiomer, *R*-warfarin does not form hydrogen bonds with substrate channel residues; its interactions are primarily hydrophobic, specifically with L75, V78, L437, and T438 (Fig. 5; Table S2).

Statins (or 3-hydroxy-3-methyl-glutaryl-CoA reductase inhibitors) such as lovastatin are substrates of CYP3A4 but are competitive inhibitors themselves of CYP2C9 (56). Oxidation of lovastatin can occur at C6 or C3′ (57), but only the hydroxylated product, 6β-hydroxy lovastatin, and oxidized product, 6-exomethylene lovastatin, were obtained using PM/E143G and PM/E143G/E64G variants (58). Unlike the other drugs discussed in this section, lovastatin is neutral at physiological pH. Its hydrophobic contacts in PM include L75, A330, L437, and T438 (Fig. 5; Table S2). Hydrogen bonding of the hydroxyl substituent in the lactone ring with S72 was short lived (~22 ns), as it eventually formed interactions with solvent molecules. These interactions were also observed in the shorter (5 ns) MD simulations of lovastatin complexes of PM/E143G and PM/E143G/E64G (58). This suggests that this hydrogen bonding interaction may not play a significant role in defining ligand binding orientation or affinity.

The MD simulations suggest that, for acidic drug molecules, residues S72 in helix B′ and K69 in β-sheet 1 in $P450_{BM3}$ generally play a role in substrate recognition and product regiospecificity, analogous to R108 in CYP2C9 (59). The crystal structure of CYP2C9 in complex with a similar substrate, flurbiprofen (PDB: 1R9O (59)), has the carboxylate group buried within the active site cavity and held by a salt bridge with R108, which is located in the B-C loop (equivalent to helix B′ in $P450_{BM3}$). Unfortunately, the crystal structure of *S*-warfarin in complex with CYP2C9 (PDB: 1OG5 (54)) provides no information on

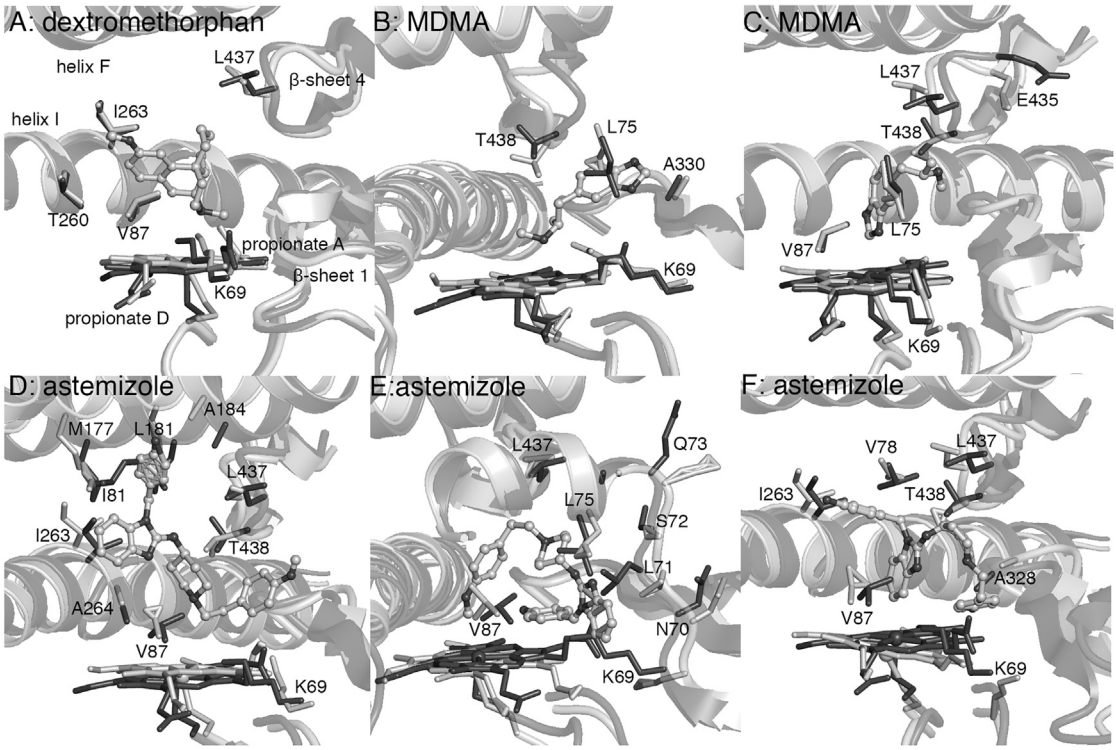

FIGURE 6 MD-averaged structures (*light gray*) superimposed on the PM-palmitic acid crystal structure (PDB: 4ZFB (20), *dark gray*). The substrates are positioned for N-dealkylation in (*A*), (*B*), and (*D*), O-dealkylation in (*C*) and (*E*), and C-H hydroxylation (C6) in (*F*).

the active site residues critical to the binding of this drug class because the substrate is bound in a nonproductive position (C7 is more than 10 Å from the oxygen binding site). The interactions with either S72 or K69 identified by this current simulation would account for the favorable net electrostatic energy that contributes to the negative ΔG_b° for naproxen and *S*-warfarin binding in PM (Fig. S5).

CYP2D6 substrates

CYP2D6 is responsible for the metabolism of ~25% of clinical drugs despite constituting <2% of hepatic CYPs (60). Typical substrates, such as antihistamines and amphetamines, contain a protonated basic nitrogen at physiological pH and planar aromatic ring (60,61). The major pathway for metabolism for these classes of molecules is O-dealkylation (62–64). Two negatively charged residues in the active site, E216 and D301, are responsible for substrate specificity and product regioselectivity (65,66).

In the absence of such residues in the $P450_{BM3}$ active site, the protonated nitrogen of dextromethorphan, MDMA, and astemizole forms an ionic interaction with heme propionate A. This positions the substrates for N-dealkylation, a reaction mainly catalyzed by a different human P450, CYP3A4 (67); N-demethylation is the second main

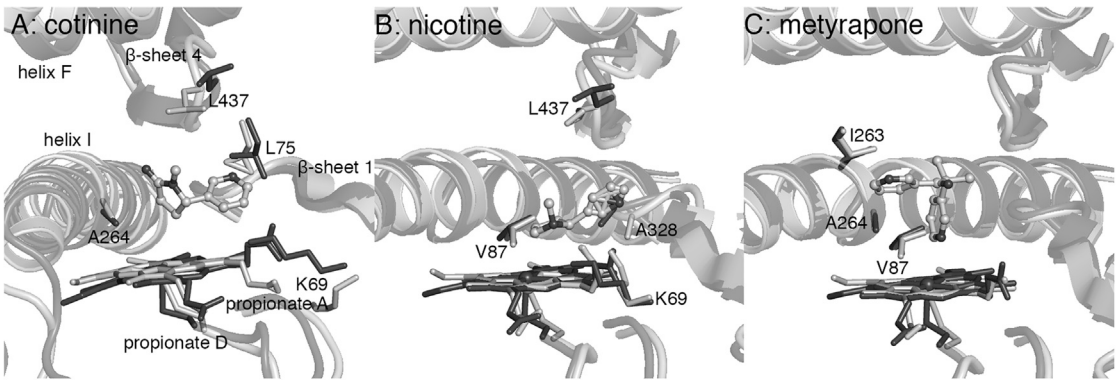

FIGURE 7 MD-averaged structures (*light gray*) superimposed on the PM-palmitic acid crystal structure (PDB: 4ZFB (20), *dark gray*). (*A*) Cotinine and (*B*) nicotine are positioned for oxidation at C5′ and C3′/C4′, respectively. (*C*) Metyrapone acts as an inhibitor by forming a covalent bond with the heme iron.

metabolic pathway for these three molecules. Experiments confirm that 3-methoxymorphinan and 3,4-methylenedioxyamphetamine are the major metabolites for dextromethorphan and MDMA, respectively, from oxidation by $P450_{BM3}$ variants containing some or all of the PM substitutions such as M01, M02, and M05 (Table 1) (8). The N-dealkylation product of astemizole, norastemizole, is a minor product of CYP3A4 metabolism (64,68) and has only been obtained so far using chimeras of $P450_{BM3}$ with other enzymes from the CYP102A subfamily (5). Hydrophobic contacts in the active site are V87, T260, I263, and L437 for dextromethorphan; L75, A330, and L437 for MDMA; and V87, L181, I263, A264, L437, and T438 for astemizole (Fig. 6; Table S3). A pronounced structural rearrangement was observed in the case of astemizole; helix F (M177, L181, A184) moved away from the protein core to accommodate the fluorophenyl ring. This would also account for the large repulsive contribution to the binding free energy (Fig. S5). A suitable orientation for N-demethylation was not observed in the simulation.

The substrate-binding pose leading to O-dealkylation was found for MDMA and astemizole (Fig. 6). The protonated nitrogen of MDMA forms a hydrogen bond with the backbone oxygen of L437 (Table S5), bringing it closer to E435 for ionic interaction. On the other hand, the benzimidazole ring of astemizole extends toward the loop connecting β-sheet 1–5 and helix B′, causing a slight distortion in this region (residues 69–74) and breaking the heme propionate A-K69 salt bridge at different points during the simulation. MDMA forms favorable hydrophobic contacts with L75, V87, L437, and T438, and astemizole mainly with L75, V87, and L437 (Table S3). In modeling the formation of another metabolite obtained with CYP2D6, 6-hydroxyastemizole (64), astemizole is forced into a folded conformation within the PM active site. The methoxyphenyl ring displaced the entire β-sheet 1, causing the heme propionate A-K69 salt bridge to break as well (Fig. 6). Hydrophobic contacts of astemizole in this binding pose include V78, V87, I263, A328, L437, and T438 (Table S3). CYP2D6 metabolites of astemizole (desmethylastemizole and 6-hydroxyastemizole; note that these reactions occur at aromatic rings at opposite ends of the large drug molecule) have been obtained with the 9-10A/A78F and 9-10A/A78F/A82G/A328F variants of $P450_{BM3}$ (Table 1) (5). The A78F and A82G substitutions, presumably, conferred greater flexibility to helix B′, allowing the enzyme to easily accept this large drug molecule in different binding orientations without causing the disruption of structure observed in simulations of PM.

CYP2A6 substrates

CYP2A6 has relatively narrow substrate specificity but has gained interest because of its involvement in the metabolism of toxic and procarcinogenic compounds (69). The crystal structure of the nicotine complex of CYP2A6 (PDB: 4EJJ (70)) indicates that F209 and I300 play a role in substrate orientation within the active site. However, nicotine does not form hydrogen bond interactions with any active site residues; its pyridine nitrogen is too far from N297, a conserved residue in CYP2A enzymes. In the PM $P450_{BM3}$ active site, the protonated nitrogen of nicotine forms an ionic interaction with heme propionate A (Fig. 7), similar to the CYP2D6 substrates. Significant hydrophobic contacts of nicotine include V87, A328, and L437 (Table S4). The major metabolite of nicotine, cotinine, is positioned for 3′- or 4′-hydroxylation in the active site (Fig. 7). Cotinine is known to be further metabolized to *trans*-3′-hydroxycotinine, the major urinary metabolite of nicotine, by CYP2A6 and CYP2A13 (71,72). In the simulation, cotinine is held by hydrophobic interactions with L75, A264, and L437 (Table S4), which orient it for reaction. Unlike nicotine and cotinine, the P450 inhibitor metyrapone, which also contains a pyridine ring, interacts primarily through formation of a coordinative bond to the heme iron. This binding mode is consistent with its role as a P450 inhibitor. Metyrapone is not subject to oxidative metabolism by P450s; rather, it undergoes reductive metabolism to form the alcohol, metyrapole, before glucuronide conjugation (73).

Factors contributing to uncoupling

Low turnover number and coupling efficiency are often observed with oxidation of non-native substrates by $P450_{BM3}$ variants. This may be attributed to catalytic uncoupling (13,14). The two major pathways for this alternative reaction pathway are 1) protonation of the proximal oxygen in the ferric hydroperoxide complex to release H_2O_2 (peroxide uncoupling) and 2) two-electron reduction and diprotonation of oxygen in the oxoferryl porphyrin radical intermediate (compound I) to yield a second water molecule (oxidase uncoupling) (Fig. 1) (15).

An experimental study of the mechanisms of the different uncoupling modes in $P450_{cam}$ indicates that excess water in the active site plays an important role in both pathways by acting as a proton source. Moreover, for peroxide uncoupling, charge separation at Fe during dissociation of HOO^- is favored by the increased polarity of the environment. Water is also thought to destabilize the ferric hydroperoxide complex by disrupting its putative hydrogen bond with a threonine residue in the active site (T268 in $P450_{BM3}$) (74). Fig. 8 shows high water density in the substrate channel when dextromethorphan, MDMA, astemizole, diclofenac, or warfarin is bound, in contrast to when palmitic acid is bound (Fig. S6). This may be attributed to the positioning of hydrophilic groups of these molecules deep within the cavity. Moreover, high water density near T268, where the hydroperoxo ligand would be bound, was observed when dextromethorphan, MDMA, and astemizole are oriented for N-dealkylation. This would be consistent

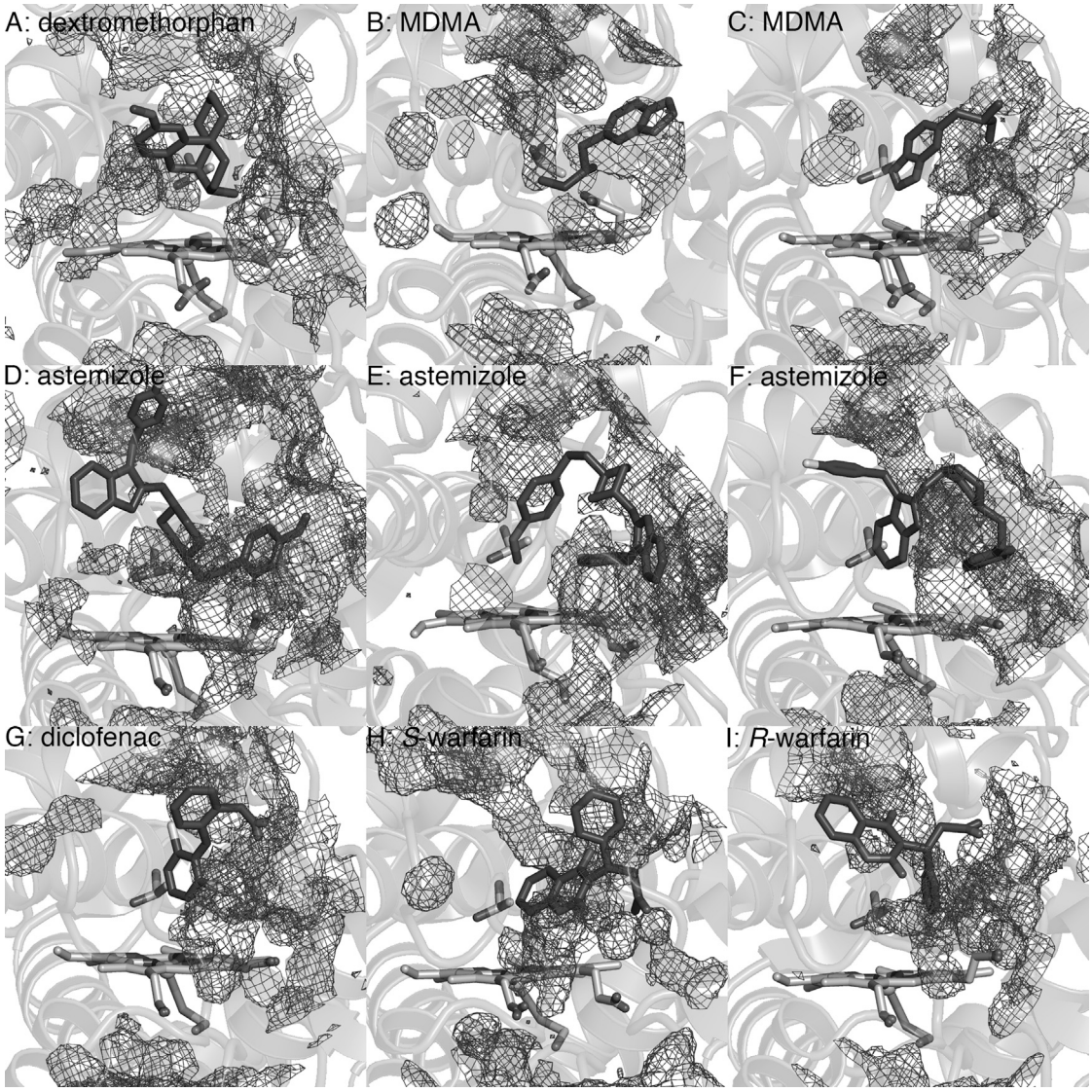

FIGURE 8 Water density at the PM $P450_{BM3}$ substrate channel, with the reference structure averaged from the MD simulation. (*A*) Dextromethorphan is positioned for N-dealkylation. MDMA is positioned for N- and O-dealkylation in (*B*) and (*C*). Astemizole is positioned for N- and O-dealkylation in (*D*) and (*E*) and C-H hydroxylation in (*F*). (*G*) Diclofenac, (*H*) *S*-warfarin, and (*I*) *R*-warfarin are positioned for C-H hydroxylation. T268, located at the distal side of the heme (helix I) and believed to play a role in proton delivery and oxygen activation, is also shown. Water density is relatively lower in the presence of palmitic acid, naproxen, lovastatin, nicotine, and cotinine (Fig. S6).

with the relatively low fraction of high-spin protein found with the PM-dextromethorphan complex (Table 2), which indicates that there is room for excess water around the heme iron even in the presence of this large substrate.

In oxidase uncoupling, electron transfer to Compound I competes with substrate oxidation. This likely occurs if the substrate is too mobile and/or the reacting atom is too distant from the oxidizing species, a consequence associated with lack of complementarity within the active site (75). The MD-averaged structures show that the shape of the PM $P450_{BM3}$ active site, meant to accommodate long-chain fatty acids, is essentially unaltered in the presence of drug molecules (Figs. 5, 6, and 7). Thus, small substrates or those that do not form stable ionic/hydrogen bond interactions with active site residues would be highly mobile during the simulations, as was the case with astemizole, diclofenac, lovastatin, cotinine, and *R*-warfarin (Fig. S7).

Reducing substrate mobility and water access to the active site can be achieved by substituting smaller active site residues with leucine, isoleucine, methionine, or phenylalanine (74). β-sheet 1–4 (residues 329–336) offers a promising mutation site for $P450_{BM3}$ because substitution with large residues would not hinder substrate access to the oxidizing heme intermediate. For example, variants containing tryptophan at position 330 within β-sheet 1–4 had high conversion rates for chlorzoxazone and lidocaine (7). On the other hand, the A330P mutation (PDB: 3M4V (24)) was found to reduce the size of the cavity by displacing the

side chain of the adjacent P329 into the active site. A330P-containing variants exhibited improved coupling efficiencies for the oxidation of small alkanes and aromatic compounds (24) and high conversion rates for naproxen, chlorzoxazone, and amitriptyline (7). The key is combining structural flexibility to allow for promiscuity with sufficient water exclusion to increase catalytic efficiency.

Heme interactions affecting oxidizing ability

Heme propionate groups not only play the structural role of anchoring the heme but may also be involved in regulating electrostatic interactions that are key to the catalytic reaction (76,77). Propionate A forms a salt bridge with K69, whereas propionate D forms a salt bridge with R398 and a hydrogen bond with W96 in $P450_{BM3}$. The binding of acidic and basic ligands, but not neutral ligands, disrupted these interactions. With dextromethorphan, MDMA, and nicotine oriented for N-dealkylation, propionate A bent toward the active site (dihedral angle of $\sim 60^{\circ}$) during the simulations (Figs. 6, 7, and S8) while maintaining interaction with K69 (Table S6). Propionate bending also occurred in the M01, M02, and M05 variants (substrate free and in complex with dextromethorphan and MDMA) based on resonance Raman and MD simulations (78). Hydrogen bonding between propionate A and the protonated nitrogen was observed for nicotine and MDMA (Table S6), which would facilitate electron transfer from the substrate to the porphyrin π-cation radical and then to Fe(IV) of compound I (77). Thus, basic functional groups that can interact directly with heme propionates do not seem to jeopardize catalytic reactivity.

In contrast, as discussed earlier, the acidic drugs *S*-warfarin and naproxen interact with K69 (Fig. 5), thus competing with propionate A (Table S5) for interaction with this residue. In the PM-naproxen complex, the interaction with K69 was broken during the simulation and propionate A instead forms a hydrogen bond with the backbone nitrogen of N395 (Table S6). This may reduce the oxidizing ability of compound I, which depends on the spin density localized on the porphyrin ring (77). Density functional theory calculations indicated that the salt bridge formed by heme propionates with Arg or Lys stabilizes the cationic porphyrin radical by weakening charge donation from the carboxylate group (76,79). Interaction with K69 could explain the low activity of most $P450_{BM3}$ variants toward acidic substrates (7,12). Introducing another hydrogen-bond-forming residue in the active site to interact with acidic substrates would therefore improve activity, as appears to be the case with the MT35 variant (Table 1), which contains the L437S substitution (10).

CONCLUSIONS

$P450_{BM3}$ variants are capable of metabolizing a wide variety of non-native substrates and have been the subject of extensive protein engineering efforts. The resulting enzymes typically contain mutations far from the active site that increase the flexibility of the lid domain without significantly altering the active site architecture. To better understand the features that regulate binding, key molecular interactions that impact substrate positioning, and factors that impact catalytic efficiencies, we performed an investigation combining experimental and computational analyses of diverse small molecules that bind to $P450_{BM3}$.

Structurally different and highly polar human P450 substrates and inhibitors were chosen for the analysis. These molecules contain acidic, basic, and polar groups and aromatic and aliphatic ring systems, and they range in molecular weight from 162.2 to 458.6 AMU (Figure 3). Despite the chemical diversity, all molecules nevertheless exhibit strong affinity for PM $P450_{BM3}$ primarily because of dispersion interactions, specifically with L75 in helix B′, I263 in helix I, L437 and T438 in β-sheet 4, A328, and V87 (Figure 2). In addition, acidic drug molecules form electrostatic interactions with S72 in helix B′ and K69 in β-sheet 1 and basic drug molecules engage with heme propionate A. However, the lack of structural and electrostatic complementarity between non-native substrates and the active site would have an impact on the turnover number and coupling efficiency of $P450_{BM3}$ variants. The resulting increase in substrate mobility and water access to the active site could lead to uncoupling reactions. Substrate interaction with K69, which forms an important salt bridge with the heme, could lessen the oxidizing ability of the enzyme. Protein-engineering efforts to develop more active and efficient $P450_{BM3}$ variants should therefore focus on reducing these effects.

SUPPORTING MATERIAL

Eight figures, six tables, and one data file are available at http://www.biophysj.org/biophysj/supplemental/S0006-3495(18)30980-9.

AUTHOR CONTRIBUTIONS

I.G., E.C.G., and C.M.P. designed the study, analyzed the data, and wrote the manuscript. I.G. performed the MD simulations. C.A.D. and D.K.H. conducted the experiments and analyzed the data.

ACKNOWLEDGMENTS

This work was supported by the National Science Foundation's (NSF) Experimental Program to Stimulate Competitive Research under grant no. 1355438. C.A.D. is supported by a Research Challenge Trust Fund fellowship and by National Institute on Drug Abuse T32 Research Fellowship (NIH DA016176). Computing resources were provided by the University of Kentucky (DLX and Kingsley clusters) and the NSF Extreme Science and Engineering Discovery Environment (XSEDE), which is supported by NSF grant no. ACI-1053575 (Gordon cluster under allocation MCB090159). This material is also based upon work supported by (while C.M.P. is serving at) the NSF.

REFERENCES

1. Schroer, K., M. Kittelmann, and S. Lütz. 2010. Recombinant human cytochrome P450 monooxygenases for drug metabolite synthesis. *Biotechnol. Bioeng.* 106:699–706.
2. Di Nardo, G., and G. Gilardi. 2012. Optimization of the bacterial cytochrome P450 BM3 system for the production of human drug metabolites. *Int. J. Mol. Sci.* 13:15901–15924.
3. Noble, M. A., C. S. Miles, …, A. W. Munro. 1999. Roles of key active-site residues in flavocytochrome P450 BM3. *Biochem. J.* 339:371–379.
4. Eiben, S., L. Kaysser, …, R. D. Schmid. 2006. Preparative use of isolated CYP102 monooxygenases – a critical appraisal. *J. Biotechnol.* 124:662–669.
5. Sawayama, A. M., M. M. Chen, …, F. H. Arnold. 2009. A panel of cytochrome P450 BM3 variants to produce drug metabolites and diversify lead compounds. *Chemistry.* 15:11723–11729.
6. Di Nardo, G., A. Fantuzzi, …, G. Gilardi. 2007. Wild-type CYP102A1 as a biocatalyst: turnover of drugs usually metabolised by human liver enzymes. *J. Biol. Inorg. Chem.* 12:313–323.
7. Ren, X., J. A. Yorke, …, L. L. Wong. 2015. Drug oxidation by cytochrome P450BM3: metabolite synthesis and discovering new P450 reaction types. *Chemistry.* 21:15039–15047.
8. van Vugt-Lussenburg, B. M., E. Stjernschantz, …, J. N. Commandeur. 2007. Identification of critical residues in novel drug metabolizing mutants of cytochrome P450 BM3 using random mutagenesis. *J. Med. Chem.* 50:455–461.
9. Damsten, M. C., B. M. van Vugt-Lussenburg, …, N. P. Vermeulen. 2008. Application of drug metabolising mutants of cytochrome P450 BM3 (CYP102A1) as biocatalysts for the generation of reactive metabolites. *Chem. Biol. Interact.* 171:96–107.
10. Reinen, J., J. S. van Leeuwen, …, J. N. Commandeur. 2011. Efficient screening of cytochrome P450 BM3 mutants for their metabolic activity and diversity toward a wide set of drug-like molecules in chemical space. *Drug Metab. Dispos.* 39:1568–1576.
11. Capoferri, L., R. Leth, …, D. P. Geerke. 2016. Insights into regioselective metabolism of mefenamic acid by cytochrome P450 BM3 mutants through crystallography, docking, molecular dynamics, and free energy calculations. *Proteins.* 84:383–396.
12. Rentmeister, A., T. R. Brown, …, F. H. Arnold. 2011. Engineered bacterial mimics of human drug metabolizing enzyme CYP2C9. *ChemCatChem.* 3:1065–1071.
13. Jung, S. T., R. Lauchli, and F. H. Arnold. 2011. Cytochrome P450: taming a wild type enzyme. *Curr. Opin. Biotechnol.* 22:809–817.
14. Fasan, R. 2012. Tuning P450 enzymes as oxidation catalysts. *ACS Catal.* 2:647–666.
15. Sono, M., M. P. Roach, …, J. H. Dawson. 1996. Heme-containing oxygenases. *Chem. Rev.* 96:2841–2888.
16. Tsotsou, G. E., A. Sideri, …, G. Gilardi. 2012. Identification of mutant Asp251Gly/Gln307His of cytochrome P450 BM3 for the generation of metabolites of diclofenac, ibuprofen and tolbutamide. *Chemistry.* 18:3582–3588.
17. Di Nardo, G., V. Dell'Angelo, …, G. Gilardi. 2016. Subtle structural changes in the Asp251Gly/Gln307His P450 BM3 mutant responsible for new activity toward diclofenac, tolbutamide and ibuprofen. *Arch. Biochem. Biophys.* 602:106–115.
18. Butler, C. F., C. Peet, …, A. W. Munro. 2013. Key mutations alter the cytochrome P450 BM3 conformational landscape and remove inherent substrate bias. *J. Biol. Chem.* 288:25387–25399.
19. Whitehouse, C. J., W. Yang, …, L. L. Wong. 2011. Structure, electronic properties and catalytic behaviour of an activity-enhancing CYP102A1 (P450(BM3)) variant. *Dalton Trans.* 40:10383–10396.
20. Geronimo, I., C. A. Denning, …, C. M. Payne. 2016. Effect of mutation and substrate binding on the stability of cytochrome P450BM3 variants. *Biochemistry.* 55:3594–3606.
21. Haines, D. C., D. R. Tomchick, …, J. A. Peterson. 2001. Pivotal role of water in the mechanism of P450BM-3. *Biochemistry.* 40:13456–13465.
22. Whitehouse, C. J., S. G. Bell, and L.-L. Wong. 2012. P450(BM3) (CYP102A1): connecting the dots. *Chem. Soc. Rev.* 41:1218–1260.
23. Kitazume, T., D. C. Haines, …, J. A. Peterson. 2007. Obligatory intermolecular electron-transfer from FAD to FMN in dimeric P450BM-3. *Biochemistry.* 46:11892–11901.
24. Whitehouse, C. J., W. Yang, …, Z. Rao. 2010. Structural basis for the properties of two single-site proline mutants of CYP102A1 (P450BM3). *ChemBioChem.* 11:2549–2556.
25. Butler, C. F., C. Peet, …, A. W. Munro. 2014. Human P450-like oxidation of diverse proton pump inhibitor drugs by 'gatekeeper' mutants of flavocytochrome P450 BM3. *Biochem. J.* 460:247–259.
26. Li, H., and T. L. Poulos. 1997. The structure of the cytochrome p450BM-3 haem domain complexed with the fatty acid substrate, palmitoleic acid. *Nat. Struct. Biol.* 4:140–146.
27. Omura, T., and R. Sato. 1964. The carbon monoxide-binding pigment of liver microsomes: II. Solubilization, purification, and properties. *J. Biol. Chem.* 239:2379–2385.
28. Morris, G. M., R. Huey, …, A. J. Olson. 2009. AutoDock4 and AutoDockTools4: automated docking with selective receptor flexibility. *J. Comput. Chem.* 30:2785–2791.
29. Bayly, C. I., P. Cieplak, …, P. A. Kollman. 1993. A well-behaved electrostatic potential based method using charge restraints for deriving atomic charges: the RESP model. *J. Phys. Chem.* 97:10269–10280.
30. Jorgensen, W. L., J. Chandrasekhar, …, M. L. Klein. 1983. Comparison of simple potential functions for simulating liquid water. *J. Chem. Phys.* 79:926–935.
31. Hornak, V., R. Abel, …, C. Simmerling. 2006. Comparison of multiple Amber force fields and development of improved protein backbone parameters. *Proteins.* 65:712–725.
32. Shahrokh, K., A. Orendt, …, T. E. Cheatham, III. 2012. Quantum mechanically derived AMBER-compatible heme parameters for various states of the cytochrome P450 catalytic cycle. *J. Comput. Chem.* 33:119–133.
33. Wang, J., W. Wang, …, D. A. Case. 2006. Automatic atom type and bond type perception in molecular mechanical calculations. *J. Mol. Graph. Model.* 25:247–260.
34. Wang, J., R. M. Wolf, …, D. A. Case. 2004. Development and testing of a general amber force field. *J. Comput. Chem.* 25:1157–1174.
35. Essmann, U., L. Perera, …, L. G. Pedersen. 1995. A smooth particle mesh Ewald method. *J. Chem. Phys.* 103:8577–8593.
36. Ryckaert, J. P., G. Ciccotti, and H. J. C. Berendsen. 1977. Numerical integration of the cartesian equations of motion of a system with constraints: molecular dynamics of n-alkanes. *J. Comput. Phys.* 23:327–341.
37. Pastor, R. W., B. R. Brooks, and A. Szabo. 1988. An analysis of the accuracy of Langevin and molecular dynamics algorithms. *Mol. Phys.* 65:1409–1419.
38. Case, D. A., V. Babin, …, P. A. Kollman. AMBER 14: University of California, San Francisco, CA.
39. Phillips, J. C., R. Braun, …, K. Schulten. 2005. Scalable molecular dynamics with NAMD. *J. Comput. Chem.* 26:1781–1802.
40. Roe, D. R., and T. E. Cheatham, III. 2013. PTRAJ and CPPTRAJ: Software for processing and analysis of molecular dynamics trajectory data. *J. Chem. Theory Comput.* 9:3084–3095.
41. Case, D. A., J. T. Berryman, …, P. A. Kollman. AMBER 2015. University of California, San Francisco.
42. The PyMOL Molecular Graphics System, Version 1.6: Schrodinger, LLC, New York.
43. Jiang, W., M. Hodoscek, and B. Roux. 2009. Computation of absolute hydration and binding free energy with free energy perturbation distributed replica-exchange molecular dynamics (FEP/REMD). *J. Chem. Theory Comput.* 5:2583–2588.
44. Shirts, M. R., and J. D. Chodera. 2008. Statistically optimal analysis of samples from multiple equilibrium states. *J. Chem. Phys.* 129:124105.

45. Isin, E. M., and F. P. Guengerich. 2008. Substrate binding to cytochromes P450. *Anal. Bioanal. Chem.* 392:1019–1030.

46. Kunze, K. L., A. C. Eddy, …, W. F. Trager. 1991. Metabolic enantiomeric interactions: the inhibition of human (S)-warfarin-7-hydroxylase by (R)-warfarin. *Chirality.* 3:24–29.

47. Poulos, T. L., and R. Raag. 1992. Cytochrome P450cam: crystallography, oxygen activation, and electron transfer. *FASEB J.* 6:674–679.

48. Sibbesen, O., Z. Zhang, and P. R. Ortiz de Montellano. 1998. Cytochrome P450cam substrate specificity: relationship between structure and catalytic oxidation of alkylbenzenes. *Arch. Biochem. Biophys.* 353:285–296.

49. Lussenburg, B. M., L. C. Babel, …, J. N. Commandeur. 2005. Evaluation of alkoxyresorufins as fluorescent substrates for cytochrome P450 BM3 and site-directed mutants. *Anal. Biochem.* 341:148–155.

50. Lin, Y. L., and B. Roux. 2013. Computational analysis of the binding specificity of Gleevec to Abl, c-Kit, Lck, and c-Src tyrosine kinases. *J. Am. Chem. Soc.* 135:14741–14753.

51. Zhou, S. F., Z. W. Zhou, and M. Huang. 2010. Polymorphisms of human cytochrome P450 2C9 and the functional relevance. *Toxicology.* 278:165–188.

52. Tang, W., R. A. Stearns, …, T. A. Baillie. 1999. Roles of human hepatic cytochrome P450s 2C9 and 3A4 in the metabolic activation of diclofenac. *Chem. Res. Toxicol.* 12:192–199.

53. Miners, J. O., S. Coulter, …, D. J. Birkett. 1996. Cytochromes P450, 1A2, and 2C9 are responsible for the human hepatic O-demethylation of R- and S-naproxen. *Biochem. Pharmacol.* 51:1003–1008.

54. Williams, P. A., J. Cosme, …, H. Jhoti. 2003. Crystal structure of human cytochrome P450 2C9 with bound warfarin. *Nature.* 424:464–468.

55. Kaminsky, L. S., and Z. Y. Zhang. 1997. Human P450 metabolism of warfarin. *Pharmacol. Ther.* 73:67–74.

56. Transon, C., T. Leemann, and P. Dayer. 1996. In vitro comparative inhibition profiles of major human drug metabolising cytochrome P450 isozymes (CYP2C9, CYP2D6 and CYP3A4) by HMG-CoA reductase inhibitors. *Eur. J. Clin. Pharmacol.* 50:209–215.

57. García, M. J., R. F. Reinoso, …, J. R. Prous. 2003. Clinical pharmacokinetics of statins. *Methods Find. Exp. Clin. Pharmacol.* 25:457–481.

58. Kim, K. H., J. Y. Kang, …, C. H. Yun. 2011. Generation of human chiral metabolites of simvastatin and lovastatin by bacterial CYP102A1 mutants. *Drug Metab. Dispos.* 39:140–150.

59. Wester, M. R., J. K. Yano, …, E. F. Johnson. 2004. The structure of human cytochrome P450 2C9 complexed with flurbiprofen at 2.0-A resolution. *J. Biol. Chem.* 279:35630–35637.

60. Wang, B., L. P. Yang, …, S. F. Zhou. 2009. New insights into the structural characteristics and functional relevance of the human cytochrome P450 2D6 enzyme. *Drug Metab. Rev.* 41:573–643.

61. Rowland, P., F. E. Blaney, …, A. M. Bridges. 2006. Crystal structure of human cytochrome P450 2D6. *J. Biol. Chem.* 281:7614–7622.

62. Yu, A., H. Dong, …, R. L. Haining. 2001. Characterization of dextromethorphan O- and N-demethylation catalyzed by highly purified recombinant human CYP2D6. *Drug Metab. Dispos.* 29:1362–1365.

63. Meyer, M. R., F. T. Peters, and H. H. Maurer. 2009. The role of human hepatic cytochrome P450 isozymes in the metabolism of racemic 3,4-methylenedioxyethylamphetamine and its single enantiomers. *Drug Metab. Dispos.* 37:1152–1156.

64. Matsumoto, S., and Y. Yamazoe. 2001. Involvement of multiple human cytochromes P450 in the liver microsomal metabolism of astemizole and a comparison with terfenadine. *Br. J. Clin. Pharmacol.* 51:133–142.

65. Paine, M. J., L. A. McLaughlin, …, C. R. Wolf. 2003. Residues glutamate 216 and aspartate 301 are key determinants of substrate specificity and product regioselectivity in cytochrome P450 2D6. *J. Biol. Chem.* 278:4021–4027.

66. Wang, A., C. D. Stout, …, E. F. Johnson. 2015. Contributions of ionic interactions and protein dynamics to cytochrome P450 2D6 (CYP2D6) substrate and inhibitor binding. *J. Biol. Chem.* 290:5092–5104.

67. Coutts, R. T., P. Su, and G. B. Baker. 1994. Involvement of CYP2D6, CYP3A4, and other cytochrome P-450 isozymes in N-dealkylation reactions. *J. Pharmacol. Toxicol. Methods.* 31:177–186.

68. Sun, H., and D. O. Scott. 2011. Metabolism of 4-aminopiperidine drugs by cytochrome P450s: molecular and quantum mechanical insights into drug design. *ACS Med. Chem. Lett.* 2:638–643.

69. Xu, C., S. Goodz, …, R. F. Tyndale. 2002. CYP2A6 genetic variation and potential consequences. *Adv. Drug Deliv. Rev.* 54:1245–1256.

70. DeVore, N. M., and E. E. Scott. 2012. Nicotine and 4-(methylnitrosamino)-1-(3-pyridyl)-1-butanone binding and access channel in human cytochrome P450 2A6 and 2A13 enzymes. *J. Biol. Chem.* 287:26576–26585.

71. Murphy, S. E., L. M. Johnson, and D. A. Pullo. 1999. Characterization of multiple products of cytochrome P450 2A6-catalyzed cotinine metabolism. *Chem. Res. Toxicol.* 12:639–645.

72. Bao, Z., X. Y. He, …, J. Y. Hong. 2005. Metabolism of nicotine and cotinine by human cytochrome P450 2A13. *Drug Metab. Dispos.* 33:258–261.

73. Murata, H., T. Higuchi, and M. Otagiri. 2016. Oral pharmacokinetics and in-vitro metabolism of metyrapone in male rats. *J. Pharm. Pharmacol.* 68:970–979.

74. Loida, P. J., and S. G. Sligar. 1993. Molecular recognition in cytochrome P-450: mechanism for the control of uncoupling reactions. *Biochemistry.* 32:11530–11538.

75. Raag, R., and T. L. Poulos. 1991. Crystal structures of cytochrome P-450CAM complexed with camphane, thiocamphor, and adamantane: factors controlling P-450 substrate hydroxylation. *Biochemistry.* 30:2674–2684.

76. Guallar, V., and B. Olsen. 2006. The role of the heme propionates in heme biochemistry. *J. Inorg. Biochem.* 100:755–760.

77. Poulos, T. L. 2007. The Janus nature of heme. *Nat. Prod. Rep.* 24:504–510.

78. Stjernschantz, E., B. M. van Vugt-Lussenburg, …, C. Oostenbrink. 2008. Structural rationalization of novel drug metabolizing mutants of cytochrome P450 BM3. *Proteins.* 71:336–352.

79. Guallar, V., M. H. Baik, …, R. A. Friesner. 2003. Peripheral heme substituents control the hydrogen-atom abstraction chemistry in cytochromes P450. *Proc. Natl. Acad. Sci. USA.* 100:6998–7002.

Biophysical Journal, Volume *115*

Supplemental Information

Molecular Determinants of Substrate Affinity and Enzyme Activity of a Cytochrome $P450_{BM3}$ Variant

Inacrist Geronimo, Catherine A. Denning, David K. Heidary, Edith C. Glazer, and Christina M. Payne

Table S1. Predicted protonation states of substrates at physiological pH.[a]

Substrate	Number of titratable atoms	Strongest acidic/basic pK_a	Charge at pH 7.4
diclofenac	2	4.00	-1.00
naproxen	1	4.19	-1.00
warfarin	1	5.56	-0.99
lovastatin	1	14.91	0.00
dextromethorphan	1	9.85	1.00
MDMA	1	10.14	1.00
astemizole	2	8.73	1.02
nicotine	2	8.58	0.94
cotinine	2	4.79	0.00
metyrapone	2	4.87	0.00

[a] https://chemicalize.com (accessed April 2018)

Table S2. Van der Waals component of pairwise interaction energy (kcal/mol) for diclofenac (DIF), naproxen (NPS), *S*-warfarin (SWF), *R*-warfarin (RWF), and lovastatin (LVA) complexes. Mean and standard deviation were calculated by averaging over 5-ns blocks.

Residue	DIF	NPS	SWF	RWF	LVA
S72	0.14 ± 0.57	1.02 ± 0.20	-0.54 ± 0.12	-0.18 ± 0.15	-0.76 ± 0.25
A74	-1.23 ± 0.20	-0.44 ± 0.08	-1.17 ± 0.04	-0.77 ± 0.17	-1.18 ± 0.36
L75	-4.20 ± 0.72	-3.60 ± 0.16	-4.05 ± 0.14	-2.67 ± 0.15	-3.99 ± 0.18
V78	-0.98 ± 0.10	-0.15 ± 0.01	-1.04 ± 0.05	-3.86 ± 0.20	-1.64 ± 0.12
V87	-2.50 ± 0.32	-1.71 ± 0.22	-3.01 ± 0.10	-2.19 ± 0.21	-2.11 ± 0.13
L181	-0.63 ± 0.33	-0.05 ± 0.02	-0.08 ± 0.01	-0.96 ± 0.04	-1.29 ± 0.15
T260	-0.15 ± 0.01	-0.06 ± 0.01	-0.08 ± 0.01	-1.31 ± 0.27	-0.48 ± 0.13
I263	-1.21 ± 0.24	-0.27 ± 0.08	-0.19 ± 0.03	-2.07 ± 0.10	-1.31 ± 0.15
A264	-1.52 ± 0.22	-1.10 ± 0.16	-0.92 ± 0.06	-2.06 ± 0.28	-1.21 ± 0.08
V267	-0.73 ± 0.08	-0.41 ± 0.21	-0.38 ± 0.07	-0.73 ± 0.08	-1.05 ± 0.30
T268	-0.93 ± 0.07	-0.79 ± 0.09	-0.82 ± 0.02	-0.58 ± 0.07	-1.25 ± 0.12
A328	-0.55 ± 0.42	-1.50 ± 0.07	-1.62 ± 0.21	-1.21 ± 0.21	-1.04 ± 0.17
A330	-0.47 ± 0.25	-1.89 ± 0.04	-1.33 ± 0.03	-0.50 ± 0.11	-2.91 ± 0.19
M354	-0.09 ± 0.04	-0.93 ± 0.06	-0.33 ± 0.09	-0.05 ± 0.01	-1.24 ± 0.07
L437	-3.37 ± 0.64	-1.64 ± 0.17	-3.79 ± 0.13	-3.76 ± 0.10	-4.99 ± 0.54
T438	-2.32 ± 0.42	-1.26 ± 0.11	-0.94 ± 0.04	-2.47 ± 0.30	-3.30 ± 0.36

Table S3. Van der Waals component of pairwise interaction energy (kcal/mol) for dextromethorphan (DEX), MDMA, and astemizole (AST) complexes. Mean and standard deviation were calculated by averaging over 5-ns blocks.

Residue	DEX	MDMA[a]	MDMA[b]	AST[a]	AST[b]	AST[c]
S72	-0.01 ± 0.01	-0.64 ± 0.11	-0.19 ± 0.03	-0.20 ± 0.11	-1.71 ± 0.90	-0.70 ± 0.52
A74	-0.04 ± 0.01	-0.15 ± 0.02	-0.88 ± 0.07	-0.59 ± 0.12	-0.97 ± 0.63	-1.13 ± 0.46
L75	-1.48 ± 0.19	-2.24 ± 0.14	-2.02 ± 0.11	-1.48 ± 0.42	-3.86 ± 1.10	-2.40 ± 0.82
V78	-1.34 ± 0.27	-0.06 ± 0.01	-0.99 ± 0.11	-5.41 ± 0.38	-2.15 ± 0.40	-2.76 ± 0.45
V87	-3.78 ± 0.08	-1.22 ± 0.16	-2.06 ± 0.18	-1.82 ± 0.12	-5.37 ± 0.37	-3.22 ± 0.40
L181	-1.17 ± 0.34	-0.02 ± 0.01	-0.17 ± 0.06	-3.20 ± 0.41	-0.58 ± 0.29	-1.05 ± 0.16
T260	-2.20 ± 0.15	-0.04 ± 0.01	-0.13 ± 0.02	-1.71 ± 0.09	-0.27 ± 0.03	-1.12 ± 0.22
I263	-3.88 ± 0.45	-0.10 ± 0.01	-0.70 ± 0.18	-4.65 ± 0.32	-1.45 ± 0.29	-2.80 ± 0.34
A264	-1.35 ± 0.17	-0.83 ± 0.04	-1.71 ± 0.08	-3.02 ± 0.14	-1.73 ± 0.19	-2.53 ± 0.23
V267	-1.47 ± 0.55	-0.02 ± 0.01	-0.60 ± 0.14	-1.08 ± 0.09	-1.48 ± 0.53	-1.17 ± 0.08
T268	-1.59 ± 0.10	-1.10 ± 0.06	-1.12 ± 0.04	-1.54 ± 0.05	-1.37 ± 0.17	-1.15 ± 0.16
A328	-0.95 ± 0.21	-1.36 ± 0.05	-1.16 ± 0.34	-2.40 ± 0.09	-1.17 ± 0.25	-2.84 ± 0.53
A330	-0.12 ± 0.03	-2.39 ± 0.12	-0.38 ± 0.07	-1.57 ± 0.20	-0.57 ± 0.24	-1.25 ± 0.19
M354	0.00	-0.72 ± 0.05	-0.03 ± 0.01	-0.14 ± 0.03	-0.08 ± 0.05	-0.05 ± 0.01
L437	-2.33 ± 0.44	-2.65 ± 0.11	-1.94 ± 0.14	-5.22 ± 0.92	-2.60 ± 0.31	-3.86 ± 0.57
T438	-1.40 ± 0.28	-1.28 ± 0.03	-2.09 ± 0.08	-3.14 ± 0.11	-1.37 ± 0.21	-2.76 ± 0.61

[a] positioned for N-dealkylation
[b] positioned for O-dealkylation
[c] positioned for C–H hydroxylation

Table S4. Van der Waals component of pairwise interaction energy (kcal/mol) for nicotine (NCT), cotinine (CTN), and metyrapone (MYT) complexes. Mean and standard deviation were calculated by averaging over 5-ns blocks.

Residue	NCT	CTN	MYT
S72	-0.12 ± 0.04	-0.19 ± 0.05	-0.01 ± 0.01
A74	-0.04 ± 0.01	-0.10 ± 0.02	-0.04 ± 0.01
L75	-1.35 ± 0.16	-2.23 ± 0.10	-1.34 ± 0.09
V78	-0.07 ± 0.01	-0.40 ± 0.06	-1.40 ± 0.07
V87	-1.61 ± 0.12	-1.66 ± 0.05	-3.78 ± 0.08
L181	-0.04 ± 0.01	-0.08 ± 0.03	-0.91 ± 0.12
T260	-0.11 ± 0.01	-0.14 ± 0.02	-1.82 ± 0.04
I263	-0.41 ± 0.08	-1.11 ± 0.19	-2.91 ± 0.05
A264	-1.54 ± 0.06	-2.17 ± 0.17	-2.89 ± 0.07
V267	-0.11 ± 0.03	-0.20 ± 0.06	-1.15 ± 0.02
T268	-1.02 ± 0.03	-0.79 ± 0.19	-1.21 ± 0.03
A328	-1.77 ± 0.14	-1.78 ± 0.11	-0.68 ± 0.13
A330	-0.94 ± 0.15	-0.39 ± 0.04	-0.07 ± 0.01
M354	-0.05 ± 0.01	-0.02 ± 0.01	0.00
L437	-1.84 ± 0.23	-2.41 ± 0.20	-2.12 ± 0.08
T438	-1.55 ± 0.09	-1.60 ± 0.08	-1.46 ± 0.06

Table S5. Hydrogen bond occupancies of substrates.

Substrate	Residue	Occupancy (%)
diclofenac:O1	S72:OG	28
diclofenac:O2	S72:OG	12
naproxen:O1	S72:OG	98
naproxen:O1	S72:N	40
naproxen:O2	S332:N	87
naproxen:O2	K69:NZ	88
S-warfarin:O2	K69:NZ	73
MDMA:N	L437:O	61

Table S6. Hydrogen bond occupancies of heme propionate A oxygen atoms.

Substrate	Heme propionate O atom	Hydrogen bond donor	Occupancy (%)
dextromethorphan	O1A	K69:NZ	24
	O2A	K69:NZ	27
MDMA	O1A	K69:NZ	74
	O2A	MDMA:N	61
astemizole	O1A	K69:NZ	34
	O2A	K69:NZ	27
nicotine	O1A	K69:NZ nicotine:N	16 39
	O2A	nicotine:N	46
naproxen	O1A	N395:N	19
	O2A	N395:N	17
S-warfarin	O1A	K69:NZ	53
	O2A	K69:NZ	27

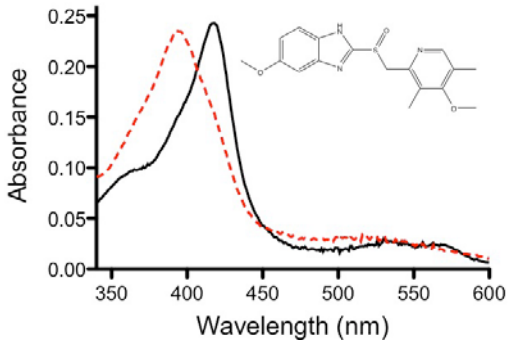

Figure S1. Absorption spectra of PM $P450_{BM3}$ bound to omeprazole (inset). The black solid curve indicates the resting, low spin state when water is bound to ferric iron. The red dotted curve represents the 100% high spin state in which water is no longer bound and omeprazole is in the active site.

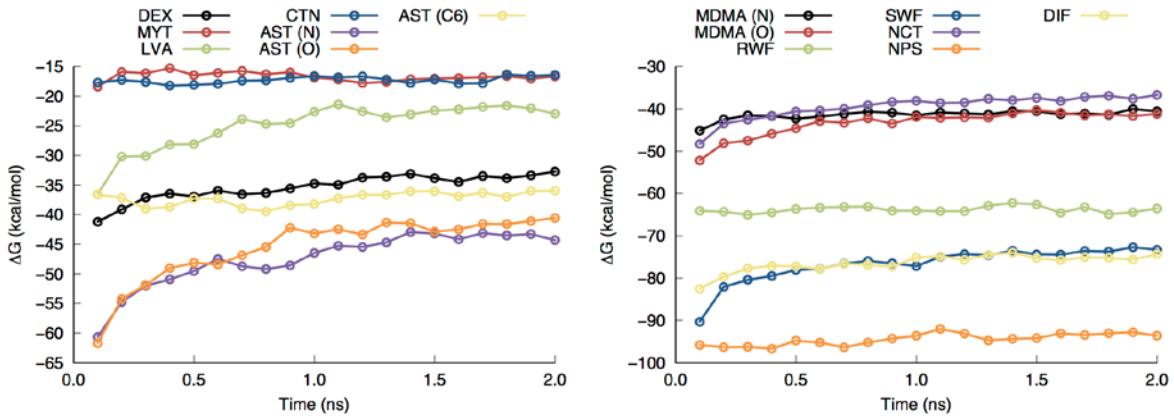

Figure S2. Gibbs free energy of the enzyme-substrate complexes during the last 2 ns of FEP/λ-REMD. The substrates are dextromethorphan (DEX), metyrapone (MYT), lovastatin (LVA), cotinine (CTN), astemizole (AST), MDMA, *R*-warfarin (RWF), *S*-warfarin (SWF), nicotine (NCT), naproxen (NPS), and diclofenac (DIF). Different binding poses were modeled for MDMA and astemizole, including N-dealkylation (N), O-dealkylation (O) and C–H hydroxylation (C6).

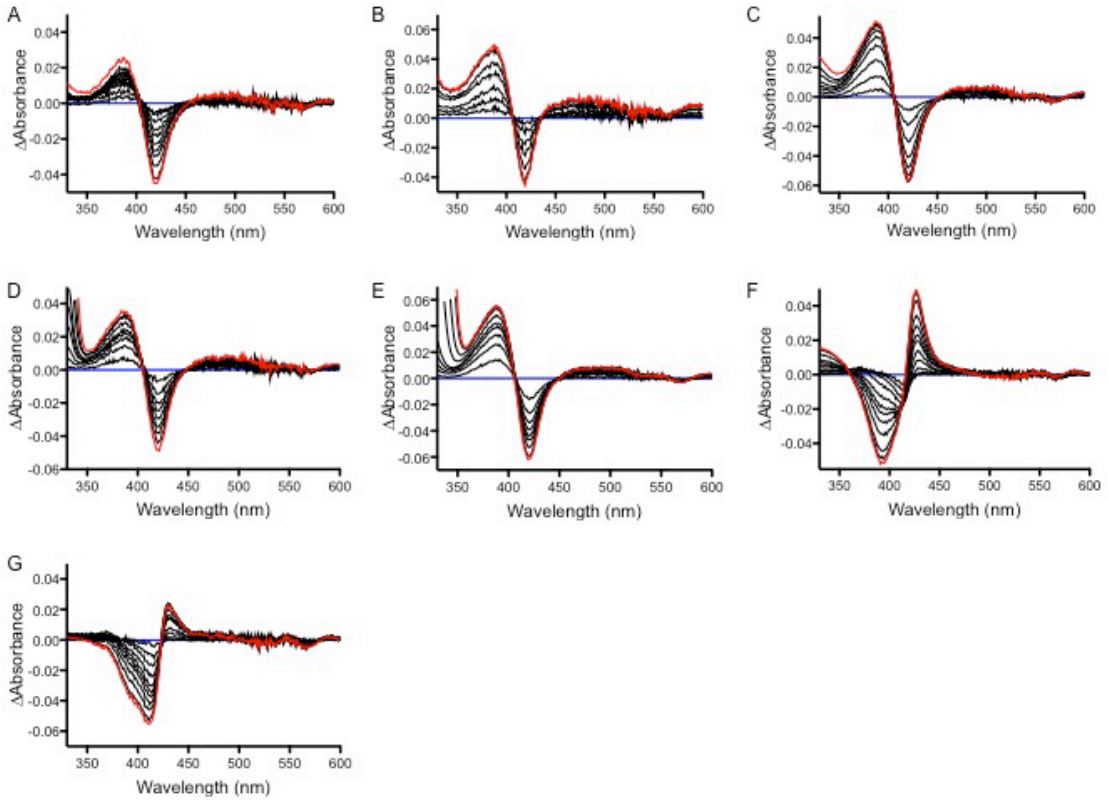

Figure S3. Difference spectra of all compounds bound to PM $P450_{BM3}$ studied experimentally. The blue line is PM $P450_{BM3}$ in which no compound is present, and the red line is fully saturated. (A) Dextromethorphan, (B) diclofenac, (C) lovastatin, (D) naproxen, and (E) racemic warfarin exhibit a type I spectral shift. (F) Cotinine and (G) nicotine exhibit a type II spectral shift.

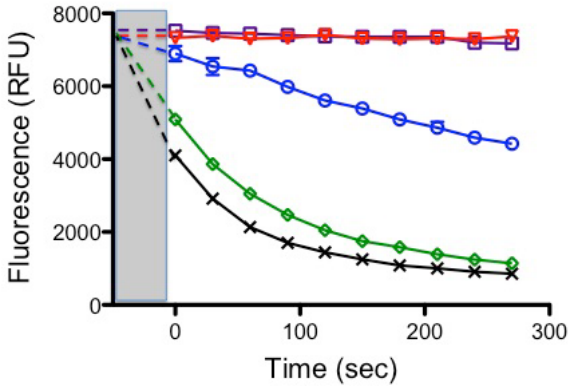

Figure S4. A 7-ethoxyresorufin-O-deethylase (EROD) activity assay was performed to determine if compounds that induced a type II spectral shift efficiently inhibited metabolism of the fluorescent substrate by PM $P450_{BM3}$. Fluorescence was monitored by excitation at 535 nm and emission at 595 nm. The gray box indicates the dead time of the instrument, and the dashed lines are projected emissions during that time (approximately 50 seconds). The black crosses indicate metabolism of 7-ethoxyresorufin when PM $P450_{BM3}$ was not inhibited. In contrast, the red triangles indicate the response when 7-ethoxyresorufin is not metabolized. Metyrapone-bound PM $P450_{BM3}$ (purple squares) was fully inhibited, whereas when cotinine was bound (green diamonds), activity was barely impacted. Interestingly, nicotine (blue circles) had an inhibitory effect on 7-ethoxyresorufin metabolism, but activity was still observed.

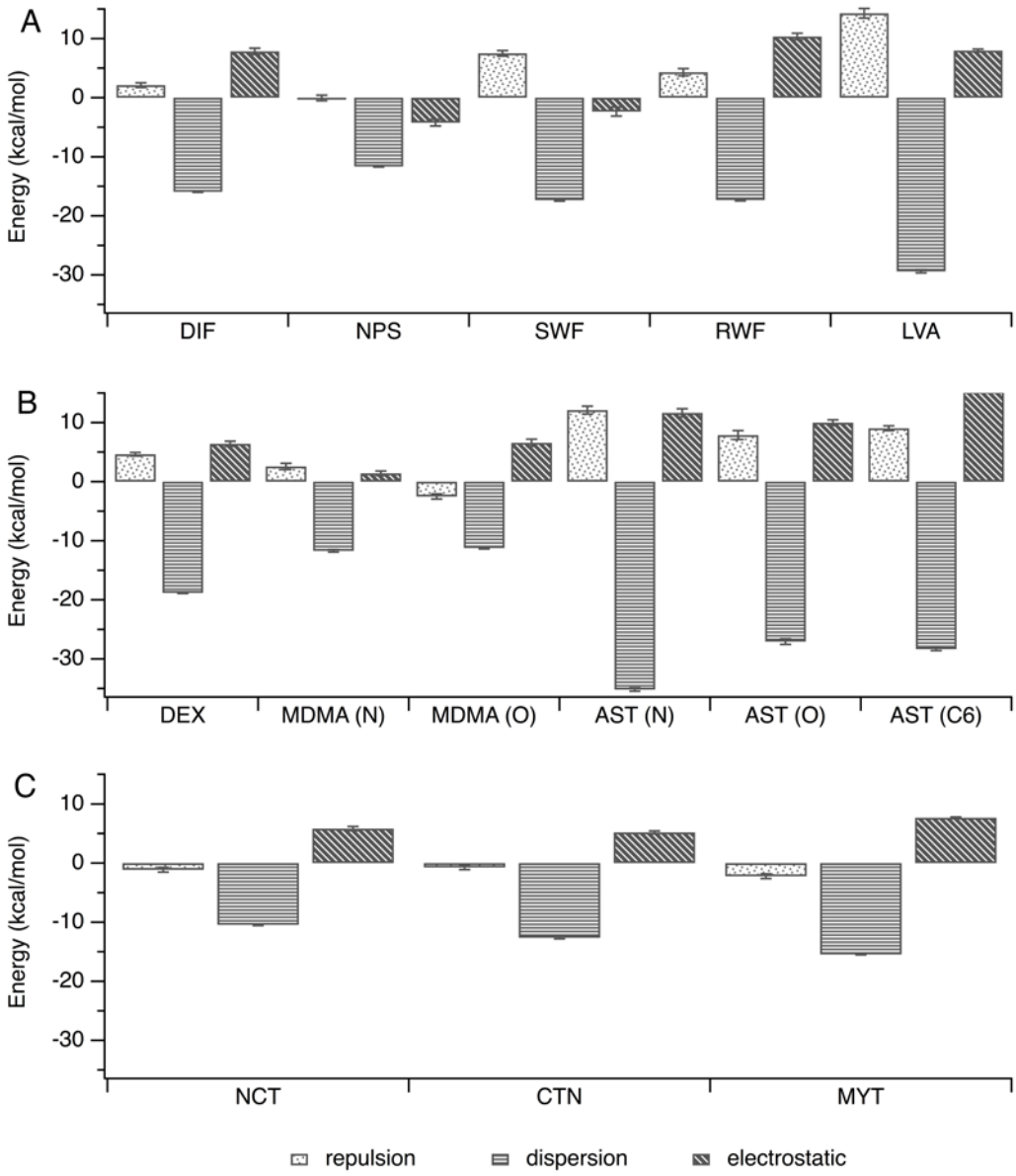

Figure S5. Repulsive, dispersive, and electrostatic energy contributions to the binding of (*A*) diclofenac (DIF), naproxen (NPS), *S*-warfarin (SWF), *R*-warfarin (RWF), lovastatin (LVA), (*B*) dextromethorphan (DEX), MDMA, astemizole (AST), (*C*) nicotine (NCT), cotinine (CTN), and metyrapone (MYT). Different binding poses were modeled for MDMA and astemizole, including N-dealkylation (N), O-dealkylation (O) and C–H hydroxylation (C6).

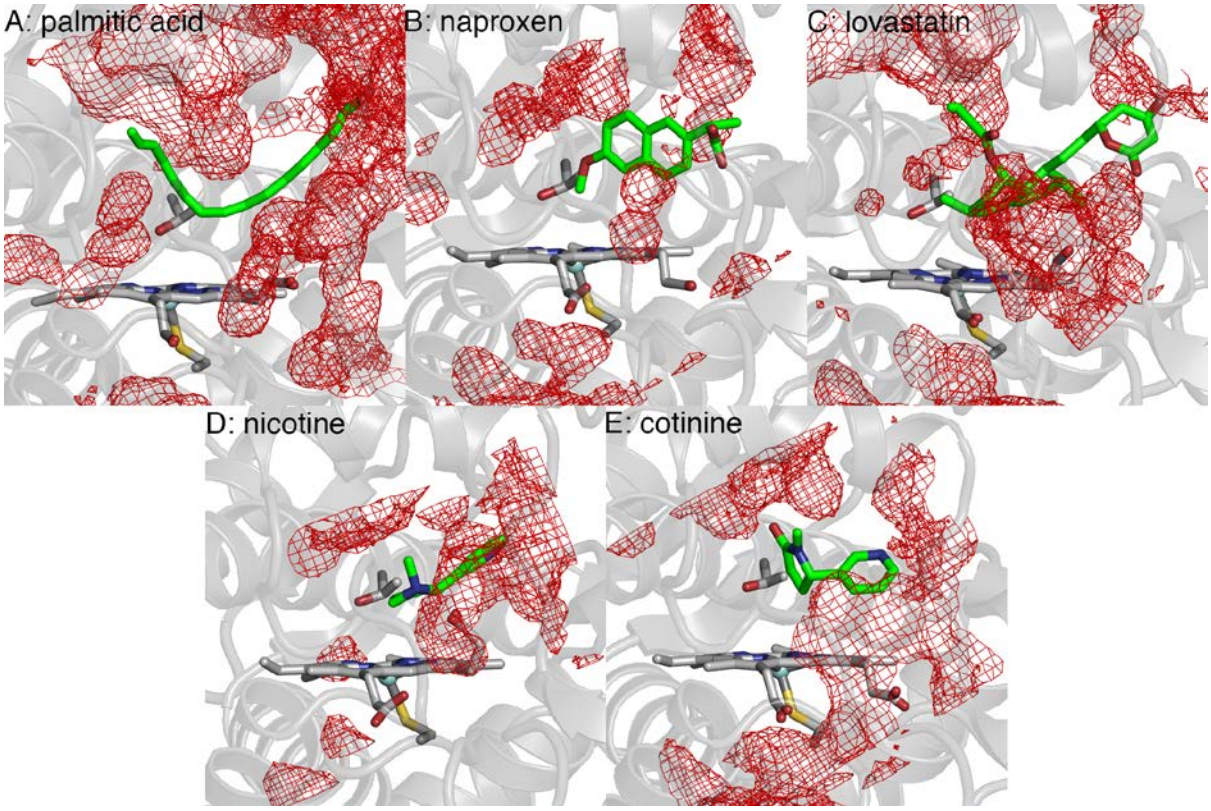

Figure S6. Water density at the PM $P450_{BM3}$ substrate channel, with the reference structure averaged from the MD simulation. T268, located at the distal side of the heme (helix I) and believed to play a role in proton delivery and oxygen activation, is also shown.

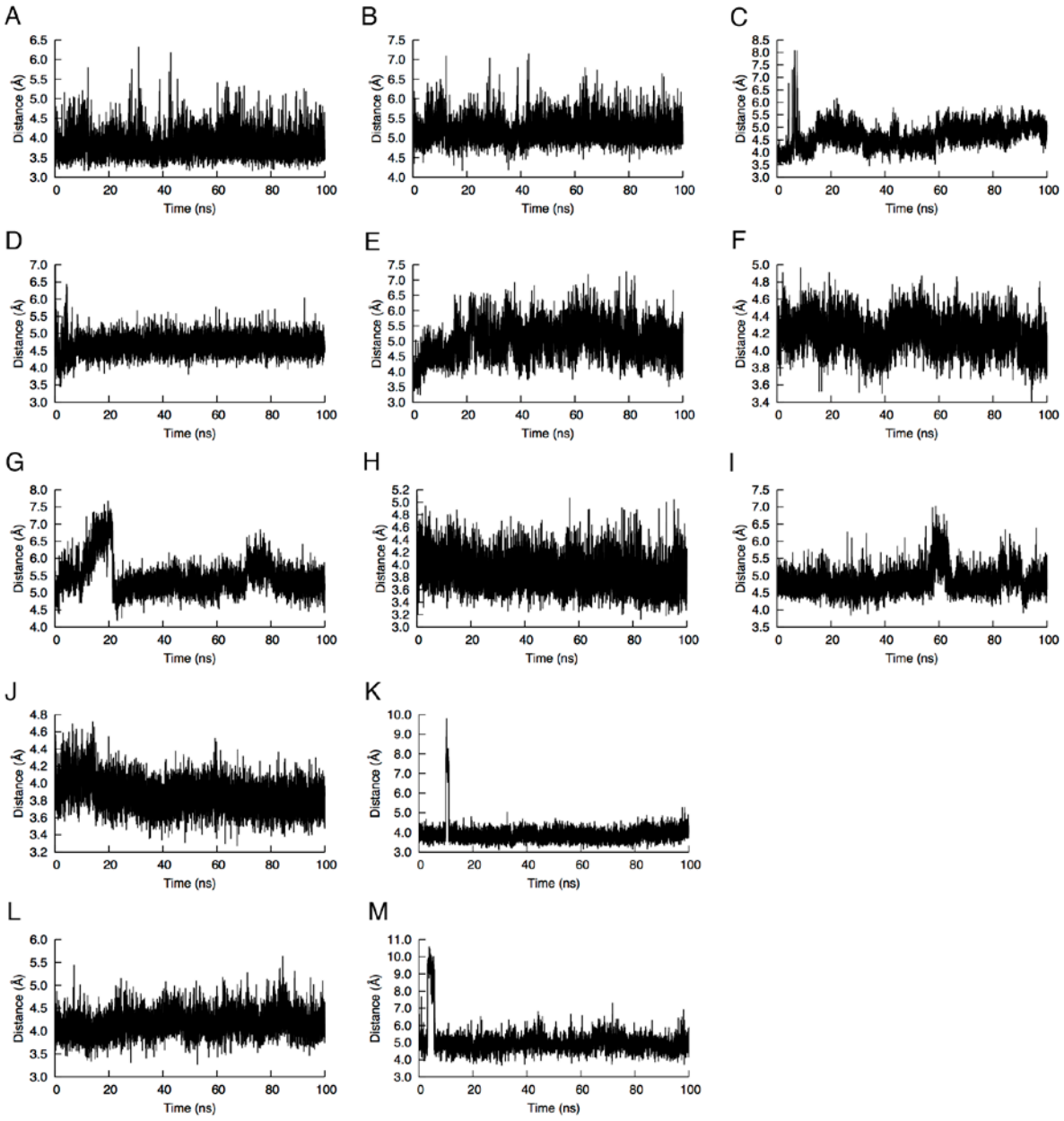

Figure S7. Plot of the distance between heme Fe and reacting atom of (*A*) diclofenac (C4'), (*B*) naproxen (methoxy C), (*C*) lovastatin (C6), (*D*) *S*-warfarin (C7), (*E*) *R*-warfarin (C4'), (*F*) dextromethorphan (protonated N), (*G–I*) astemizole (protonated N, methoxy C, C6), (*J*, *K*) MDMA (protonated N, C2), (*L*) nicotine (C5'), and (*M*) cotinine (C4').

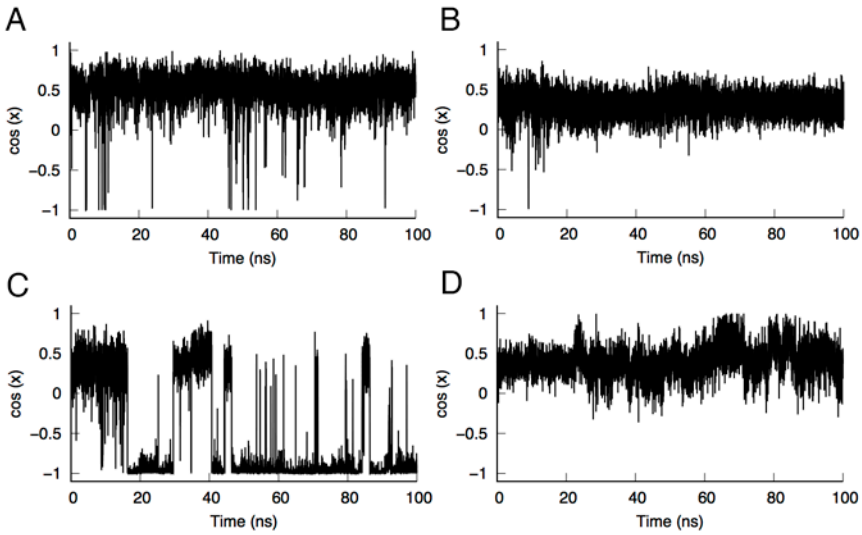

Figure S8. Plot of the cosine of the heme propionate A dihedral angle in (*A*) dextromethorphan, (*B*) MDMA, (*C*) astemizole, and (*D*) nicotine complexes of PM $P450_{BM3}$. The cosine of the dihedral angle in the PM-palmitic acid crystal structure (PDB ID: 4ZFB) is approximately -1.